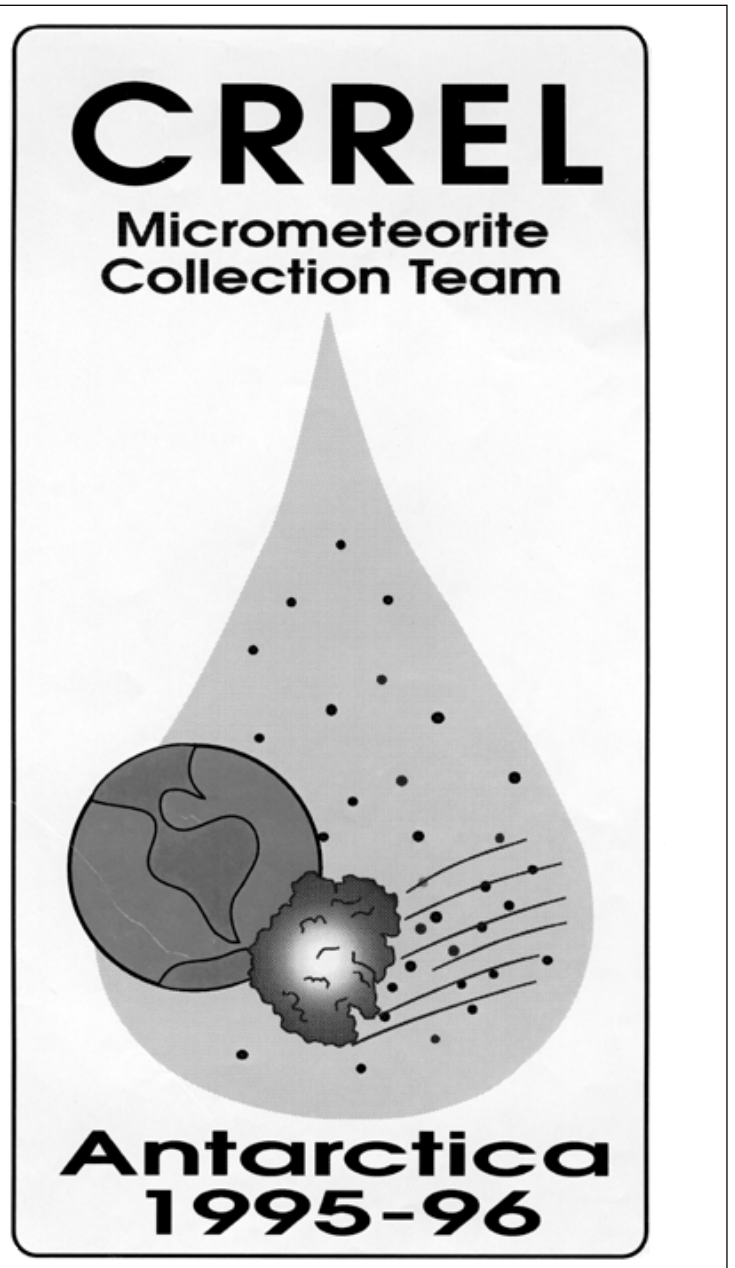
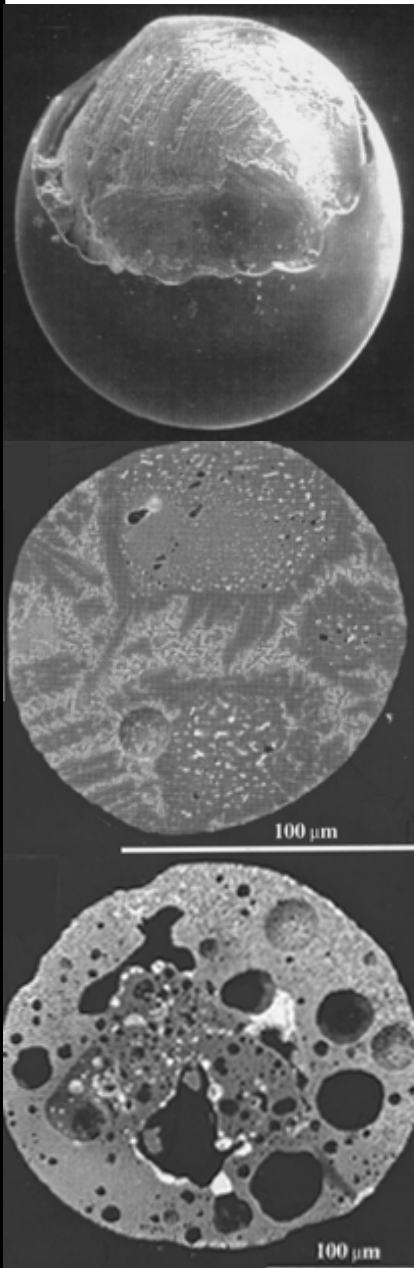




Collecting Micrometeorites from the South Pole Water Well

Susan Taylor, James H. Lever, Ralph P. Harvey, and John Govoni

May 1997



Abstract: A collector was designed and built to retrieve micrometeorites from the floor of the South Pole Water Well. The large volume of firn and ice being melted for the well and the low component of terrestrial material in Antarctic ice make the South Pole Water Well an ideal place to collect micrometeorites. Because the age of the ice being melted is known, yearly or periodic

collections provide large numbers of micrometeorites of known terrestrial age. The collector was designed to pose no threat to the well's water quality, to be reliable and easy to operate, and to collect particles larger than 50 μm . This report details how this collector was built and tested and documents the rationale behind some of the design choices. It also includes preliminary findings from the first deployment.

How to get copies of CRREL technical publications:

Department of Defense personnel and contractors may order reports through the Defense Technical Information Center:

DTIC-BR SUITE 0944
8725 JOHN J KINGMAN RD
FT BELVOIR VA 22060-6218
Telephone 1 800 225 3842
E-mail help@dtic.mil
msorders@dtic.mil
WWW <http://www.dtic.dla.mil/>

All others may order reports through the National Technical Information Service:

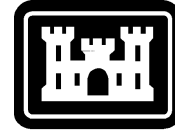
NTIS
5285 PORT ROYAL RD
SPRINGFIELD VA 22161
Telephone 1 703 487 4650
1 703 487 4639 (TDD for the hearing-impaired)
E-mail orders@ntis.fedworld.gov
WWW <http://www.fedworld.gov/ntis/ntishome.html>

A complete list of all CRREL technical publications is available from:

USACRREL (CECRL-LP)
72 LYME RD
HANOVER NH 03755-1290
Telephone 1 603 646 4338
E-mail techpubs@crrel.usace.army.mil

For information on all aspects of the Cold Regions Research and Engineering Laboratory, visit our World Wide Web site:
<http://www.crrel.usace.army.mil>

CRREL Report 97-1



**US Army Corps
of Engineers®**
Cold Regions Research &
Engineering Laboratory

Collecting Micrometeorites from the South Pole Water Well

Susan Taylor, James H. Lever, Ralph P. Harvey, and
John Govoni

May 1997

Prepared for
OFFICE OF THE CHIEF OF ENGINEERS

Approved for public release; distribution is unlimited.

PREFACE

This report was prepared by Susan Taylor, Research Physical Scientist, Geological Science Division; James Lever, Mechanical Engineer, Ice Engineering Research Division; and John Govoni, Physical Science Technician, Snow and Ice Division; of the Research and Engineering Directorate of the U.S. Army Corps of Engineers Cold Regions Research and Engineering Laboratory; and Ralph Harvey, Senior Research Associate, Department of Geological Sciences, Case Western Reserve University, Cleveland, Ohio.

Funding for this work was provided by the National Science Foundation. The report was technically reviewed by John Rand and Stephen Ackley of CRREL.

The authors wish to thank the following people who assisted in this study: Robert Forrest, William Birch, and Peter Alekseiunas, who made the components for the micrometeorite collector at CRREL; Michael Walsh, who suggested the technique for fabricating the collector arm; Dennis Lambert, who turned our ideas into detailed drawings and added improvements of his own; John Rand, who provided invaluable information about the well and the wellhouse; the CRREL brainstorming participants—Dr. Thomas Jenkins, Janet Hardy, Dr. Edgar Andreas, Deborah Diemand, Stephen Flanders, Capt. Jeffrey Wilkinson, John Rand, and Dr. J.-C. Tatinclaux—for their wonderful and varied suggestions for the collector design; Dr. Ellen Mosley Thompson, The Ohio State University, who kindly provided unpublished data on particle size distributions obtained from a South Pole core; Peter Stark, who constructed the wooden well shape on which the collectors were tested; Thomas Vaughan for his illustrations; and Jesse Stanley, who juggled his basin tests so that these tests could be run at all hours of day and night. The authors also thank Ms. Hodgdon's 8th-grade math class at Lebanon Junior High School, Lebanon, N.H., who designed the logo for the project, shown on the cover of this report. Last but not least, the authors thank Michael Shandrick, who assisted them at the Pole during the marathon drilling session and any other time his help was needed, for his dedication and good spirit.

The contents of this report are not to be used for advertising or promotional purposes. Citation of brand names does not constitute an official endorsement or approval of the use of such commercial products.

CONTENTS

	Page
Preface	ii
Introduction	1
South Pole Water Well	2
Collector design	4
Technical objectives	4
Design requirements and performance criteria	4
Preliminary design	5
Particulate concentrations expected	6
Pumping requirements and preliminary tests	7
Final design	8
Prototype tests and modifications	10
Deployment	13
Samples	15
Weathering	18
Flux rates	18
Conclusion	21
Literature cited	22
Appendix A: SPWW dimensions	25
Appendix B: Summary of collector development tests	35
Appendix C: Summary of collector deployments in SPWW	37
Abstract	39

ILLUSTRATIONS

Figure

1. Evolution of the South Pole Water Well	3
2. Approximate size and shape of the South Pole Water Well in December 1995	4
3. Original collector concept	5
4. Number and size distribution of particles >50 μm estimated for the bottom of the SPWW	6
5. Final collector-arm cross-section	8
6. Major components of the 1.2-m operational collector	9
7. Schematic of the 1.2-m collector in the SPWW	10
8. 2.5-m operational collector suspended from the cable on a winch	11
9. Slot width measured along the 1.2-m collector prior to deployment	13
10. Work space at the SPWW, consisting of a winch room directly over the access hole and an adjoining laboratory	14
11. Hot-water drill used to drill second access hole to the SPWW	14
12. Map of the bottom of the SPWW showing the plateau area and pocket no. 1	15
13. An assortment of spherules from the SPWW	16
14. Sediment retrieved from the well	17
15. Backscattered electron photomicrographs of selected SPWW micrometeorites	19
16. Ternary diagram illustrating where the analyzed SPWW spherules plot in relation to the Deep Sea and Greenland spherules	20
17. Weight percent Al/Si and Ca/Al plot of the SPWW spherules as compared to DSS and chondritic value	20
18. Photomicrograph showing a glass rind around a stony spherule	21

TABLES

	Page
Table	
1. Other wells built in polar regions	2
2. Summary of quantitative collection efficiency tests	11
3. Size range and weight of the pocket and plateau samples	17
4. Types of extraterrestrial particles in the pocket sample	18
5. Comparison of SPWW spherule types with those found in Greenland and in the Deep Sea collection	20

Collecting Micrometeorites from the South Pole Water Well

SUSAN TAYLOR, JAMES H. LEVER, RALPH P. HARVEY, AND JOHN GOVONI

INTRODUCTION

Micrometeorites are the dominant mass contribution to the present-day Earth and add one hundred tons of material to the Earth each day (Brownlee 1981, Love and Brownlee 1993). Although ubiquitous in terrestrial environments, relatively little of this material has been collected because micrometeorites occur in low concentrations and generally weather rapidly. To collect micrometeorites one needs to find deposits where they are concentrated. Like meteorites, micrometeorites range from unaltered primordial materials to those that have seen extensive differentiation and alteration deep within a parent body. They represent collision-produced fragments of asteroids as well as materials of cometary origin (Brownlee et al. 1993). Some of these small particles are thought to contain exotic materials, including interstellar grains and fragments of solar system materials that have no counterparts among meteorite collections (Bradley et al. 1989, Brownlee et al. 1993).

In this paper we use the word micrometeorite as a generic term referring to all types of terrestrially collected extraterrestrial debris with sizes <1 cm. Cosmic spherules refer to spherical and/or rounded particles that have been totally or partially melted by atmospheric entry. The term interplanetary dust particle (IDP) refers to the small (<50 μm) extraterrestrial particles collected in the stratosphere.

More than a century ago a few magnetic cosmic spherules were found in deep-sea sediments collected by members of the H.M.S. *Challenger* expedition (Murray and Renard 1876). Both iron and silicate spherules were found, and it was thought, especially of the iron spherules, which contained nickel in chondritic proportions, that they were of meteoritic origin. The presence of wustite in these spherules, a high-temperature iron oxide found in meteorite fusion crusts, also suggested an extraterrestrial origin for iron spherules (Marvin and Einaudi 1967). The extraterrestrial origin of the silicate spherules, which are composed of olivine, interstitial glass, and magnetite, was more difficult to prove. Major element analysis showed that

they had chondritic ratios of magnesium, silicon, and iron (Blanchard et al. 1978), but it required trace chemical analyses to show their extraterrestrial origin (Ganapathy et al. 1978).

Cosmic spherules are distinctive-looking particles and have been found in many terrestrial environments. They have been found in the swamps of Siberia (Krinov 1959), in desert sands (Fredriksson and Gowdy 1963), in beach sand (Marvin and Einaudi 1967), in deep sea sediments (Brownlee 1979), in lithified abyssal sediments exposed on land (Czajkowski et al. 1983, Jehanno et al. 1988, Taylor and Brownlee 1991), in Greenland's cryoconite and melt-water drainage basins (Maurette et al. 1986, 1987; Robin et al. 1990), and in Antarctic morainal sediments (Hagen 1988, Koeberl and Hagen 1989), aeolian debris (Harvey and Maurette 1991, Hagen et al. 1992), and ice cores (Yiou and Raisbeck 1990, Hagen et al. 1992).

Unmelted micrometeorites have also been sought and found. Interplanetary dust particles (IDPs) were collected in the stratosphere (Brownlee et al. 1977) and are routinely collected by NASA using U-2 high-flying aircraft. Larger unmelted micrometeorites were found in Greenland ice (Maurette et al. 1987), and many micrometeorites, primarily <100 μm in size, were found upon melting and sieving 100 tons of Antarctic blue ice (Maurette et al. 1991).

The South Pole Water Well (SPWW) is a 24-m-diameter by 15-m-deep melt pool 100 m below the snow surface; it supplies potable water to the Amundsen-Scott South Pole Station. Because of the large volume of ice melted, the well is the largest source of micrometeorites yet discovered. The compressed-snow polar ice preserves a record of melted and unmelted micrometeorites in an environment low in terrestrial debris, and the well provides the concentrating mechanism necessary for collecting these particles. The large pool volume and low water-injection rate produce low circulation velocities that cannot entrain micrometeorites melted out of the ice. These particles should, therefore, form a lag deposit on the well bottom. Based on this assumption, we built a collector to retrieve micrometeorites larger than 50 μm from the bottom of the well. We deployed the collector in De-

ember 1995 and did indeed recover large numbers of micrometeorites.

The SPWW represents a uniquely valuable source of micrometeorites. The age of the ice being melted is known as a function of depth (Kuivinen et al. 1982), making it possible to date the depositional age of the particles recovered. Although the SPWW does not allow horizontal (stratigraphic) control on a fine scale as do traditional cores, the large numbers of extraterrestrial particles from different time periods should allow a statistically significant study of the recent variation of cosmic dust flux at the Earth's surface. The first year's collection is an integrated sample of micrometeorites that fell to Earth between 1100 and 1500 A.D. As melting occurs predominantly in a downward (older ice) direction at a known

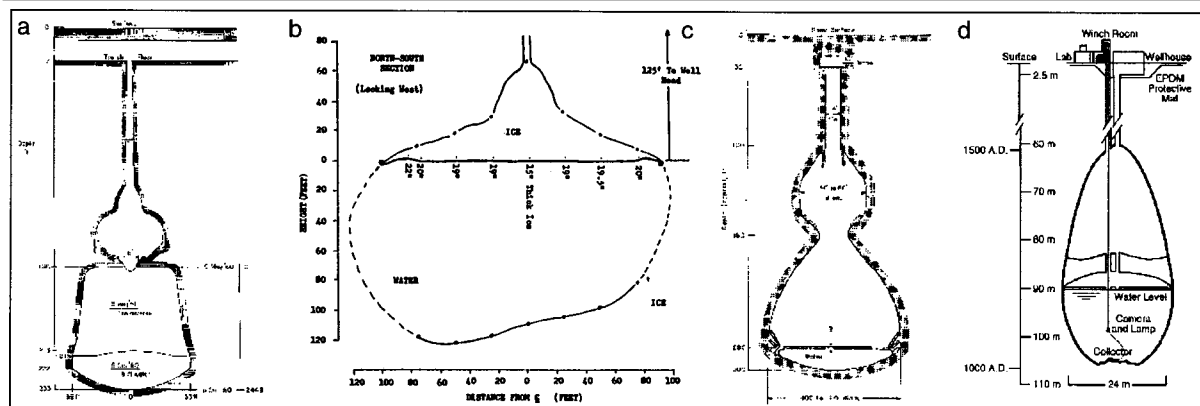
rate, later collections will be integrated samples from known depths, and thus known ages. More specifically, the well deepens approximately 10 m each year (equivalent to 100 years of deposition) and will melt ice that dates from 400 to 1500 A.D. during its life. By sampling all, or a known percentage, of the well bottom and repeating the collection on an annual basis, the flux rate and any variation in either rate or composition of micrometeorites can be determined on a 100-year time scale.

SOUTH POLE WATER WELL

In 1955 Henri Bader suggested building 'water wells' at glacier camps after observing the size and shape of sewage disposal pits (Clark 1965). Schmitt

Table 1. Other wells built in polar regions.

Date	Type	Location	Additional information
1959	Water well ^a	Camp Century, Greenland	Rodriguez assembles components and first well is made. Well reached 171.5 ft. Observer lowered into the well after most of the water had been pumped out (Schmitt and Rodriguez 1960).
1960	Water well ^a	Camp Century, Greenland	Original well is restarted, producing a 244-ft symmetrical, bell-shaped cavity (Schmitt and Rodriguez 1963).
1960-1963	Waste heat storage ^b	Camp Century, Greenland	Made from waste heat from a nuclear reactor (Clark 1965).
1960-1961	Water well	Tuto, Greenland	Russell (1965).
1964	Water well ^c	Camp Century, Greenland	Second utility well created.
1972	Water well	South Pole, Antarctica	Operated 3 months (Williams 1974).
1977-78	Drilling water	Ross Ice Shelf, Antarctica	
1990-91	Water well ^d	South Pole, Antarctica	Drilled by John Rand and John Govoni. Mined for micrometeorites in December 1995.
1994-95	Drilling water	South Pole, Antarctica	Amanda Project, PICO



and Rodriguez (1960) were the first to build a melt-pocket water well in ice, and subsequent polar wells have been called Rodriguez or Rod wells (see Table 1 for a list of such wells). Researchers have searched for cosmic spherules and extraterrestrial materials in polar wells (e.g., Langway 1963, McCorkell et al. 1970). McCorkell and his colleagues filtered 200,000 liters of water pumped from a meter from the well floor at the Camp Century well in Greenland. They found no excess ^{26}Al , an extraterrestrial marker, on their 3- μm filters. The micrometeorites had probably formed a lag deposit on the well floor, but the pump intake was too high on the well bottom to entrain the particles.

The SPWW is a Rodriguez well constructed during the 1992–93 austral summer. A hot-water drill was used to melt a 30-cm-diameter hole into the snow to a depth of 60–70 m. The drill was then lowered more slowly to create a large pool or reservoir of water. The surface wellhouse, which contains the equipment for drilling and operating the well, consists of two stacked $4.6 \times 2.1 \times 2.4$ m shipping containers (millvans). The wellhead is in the lower container, about 2.5 m below the present snow surface. The 30-cm-diam. wellhead and neck accommodate the electrical cable connected to the submersible pump, emergency heat trace, and two

insulated hoses (one carrying water to the surface and one returning warm water to the well). Because contamination of the well by fuel was a major concern, a low-temperature EPDM (ethylene propylene dienemonomer) mat surrounds the wellhead and extends out 7 m.

The SPWW was certified as a source of potable water in early 1994. On 26 February 1994, the pool was about 16 m deep and 22 m in diameter, and the well bottom was 101 m below the wellhouse (103.5 m below the snow surface, Appendix A). Before consumption began, however, an electrical fire in the pump cable on 1 March 1994 forced a 9-month shutdown. During the shutdown, a 4-m-thick ice layer formed on the pool surface and 6–11 m of freezeback occurred on the walls and bottom. The well was restarted in December 1994 by drilling through the ice layer and recirculating warm water as before. By March 1995, the well had melted below the prefire level and released any particles trapped during the freezeback. Figure 1 shows the approximate well geometry before and after the fire and at the time of deployment in December 1995. It also shows the corresponding age of the ice (and the depositional age of the micrometeorites).

The SPWW has supplied potable water since

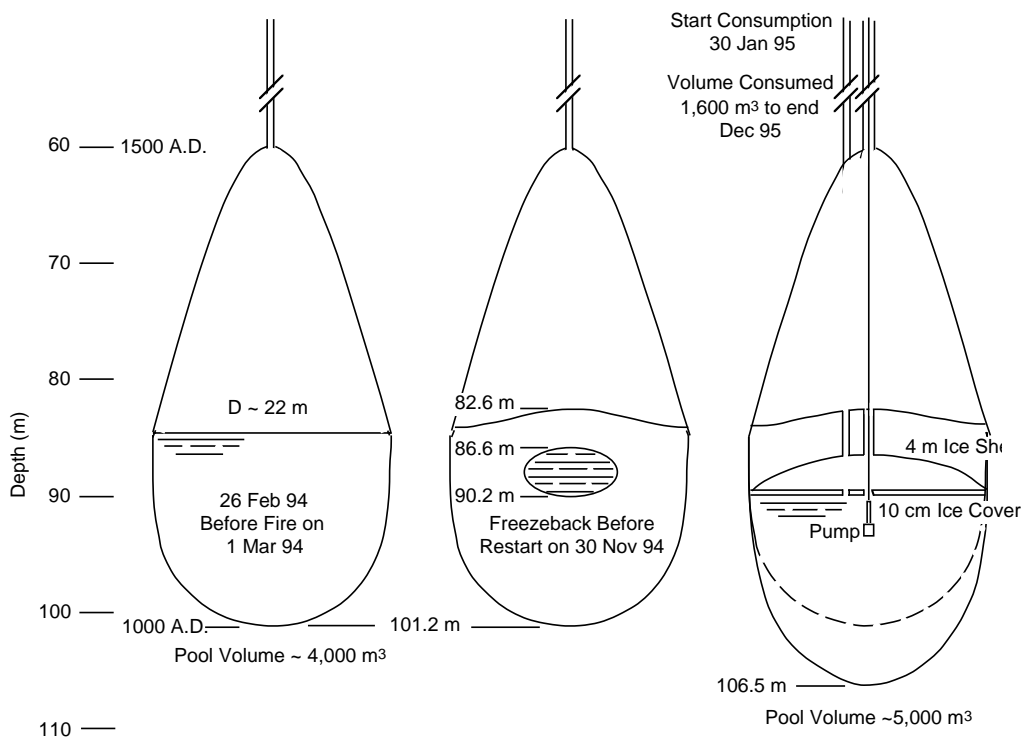


Figure 1. Evolution of the South Pole Water Well.

January 1995. The reservoir has reached a relatively stable size of about 24 m diameter and 16 m depth and contains about 5,000 m³ of water (based on water consumption and depth data, Appendix A). The present consumption rate is about 2,000 m³ (about 2 million liters) per year. The pump draws water from about 1 m below the water surface. About 10% of the water is consumed and the rest is heated, using waste heat from the station, and returned to the well.

The flow rate of returning water is about 1 L s⁻¹, and it is discharged 3 m below the water surface through a nozzle designed to produce a uniform, 90° cone-shaped jet. Peak discharge velocity 1 m away from the nozzle should be less than 1 mm s⁻¹, and no remnants of the jet should persist at the well bottom. Rather, the jet and heat input probably establish large-scale circulation cells in the pool. It seems very unlikely that circulation velocities at the well bottom would be adequate to entrain the micrometeorites of interest.

The effort required to model the flow distribution in the SPWW was beyond the scope of our work. However, we estimated the velocities needed to transport micrometeorites and assessed whether such velocities were likely to be present. To initiate movement of a 50-μm particle with a density of 2.5 g cm⁻³ (stony or glassy micrometeorites), flow velocity along the well bottom would need to exceed about 6 cm s⁻¹ (ASCE 1975). The micrometeorites of interest are generally larger or more dense and hence would have higher thresholds. It seems unlikely that bottom velocities would exceed threshold values, given that velocities 1 m from the nozzle are substantially lower. We therefore thought that micrometeorites would form a lag deposit on the well bottom as they are melted out of the ice.

Originally we had planned to deploy the collector during an annual maintenance period when the well's pump and hoses were removed for servicing.* However, space in the well house is very limited, complicating collector deployment, and our collection time would have been restricted to a few hours. For these reasons we drilled a second access hole, about 2 m from the central hole, and had a separate work area constructed (Fig. 2).

*J.H. Rand, 1996, Ice Engineering Division, CRREL, personal communication.

COLLECTOR DESIGN

Technical objectives

Our technical objectives were (a) to collect essentially all of the micrometeorites from a large, known area of the well bottom, and (b) to be capable of returning to the same area of the well bottom annually. Assuming that the micrometeorites form a lag deposit, meeting these technical objectives would allow us to calculate flux rates and document any temporal changes in the composition of the particles (i.e., meet the scientific objectives).

Design requirements and performance criteria

The nature of the SPWW imposes strict requirements on the collector design. The collector must not degrade water quality under any circumstances. It must fit down a 30-cm-diam. well neck and survive a cold soak at -50°C during its descent to the well pool. It must operate remotely in about 20 m of water at a distance of 200 m below the snow surface.

In addition, we specified several performance criteria to help guide our design selections. The collector should collect essentially all particles in

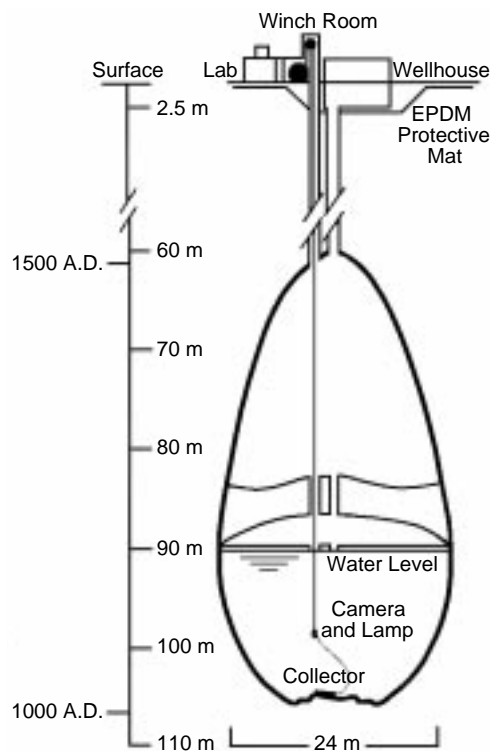


Figure 2. Approximate size and shape of the South Pole Water Well in December 1995.

the size range 50–1000 μm without bias to composition (e.g., toward magnetic particles). Its collection efficiency should be high (and we should measure it). It should cause no physical or chemical changes to the particles. Its design should minimize handling losses after collection. It should give reliable performance and be adaptable to unknown bottom surface conditions. In addition, its design should minimize the possibility of it becoming stuck in the well.

Preliminary design

We had a brainstorming session to gather preliminary collector concepts. After reviewing these ideas, we selected a concept that involved down-hole suctioning and filtering of the particles by a mobile collector controlled from the surface. Figure 3 shows this concept as originally envisioned. It utilizes the unconstrained, vertical dimension of the well neck to maximize the filter capacity and the area swept out by the collector in a single pass. A pump develops a high-speed flow to suction particles through a slot along the underside of a long, flexible arm containing a filter. The filter arm would be formed from a flexible, drinking-water-safe plastic to allow it to conform to the curved well bottom. We could drive the long arm around in a circle and measure its rotation to determine

the area swept. Separate filter chambers distributed along the arm would reveal information about the radial distribution of particles. Alternatively, we could independently operate a drive motor at either end of a shorter version of the collector to maneuver it over undulating well-bottom topography. An underwater video camera would help maneuver the collector and document the area swept.

This concept contains many advantages over alternatives considered. Suctioning particles by entraining them in a water stream should avoid any compositional bias in the collection (assuming that the water flow is high enough to entrain the heaviest particles of interest). Down-hole filtering avoids the need to pump water and particles to the surface, saving pumping requirements and avoiding particle damage and losses within the piping system. Indeed, our design minimizes particle damage and losses by incorporating the filter immediately downstream of the intake slot.

Further development of this concept required basic data on the number of particles expected (to determine filter capacity), the flow velocity needed to entrain the particles of interest, and the pumping losses expected (to size the pump). We also investigated several fabrication options to incorporate a filter into the collector arm.

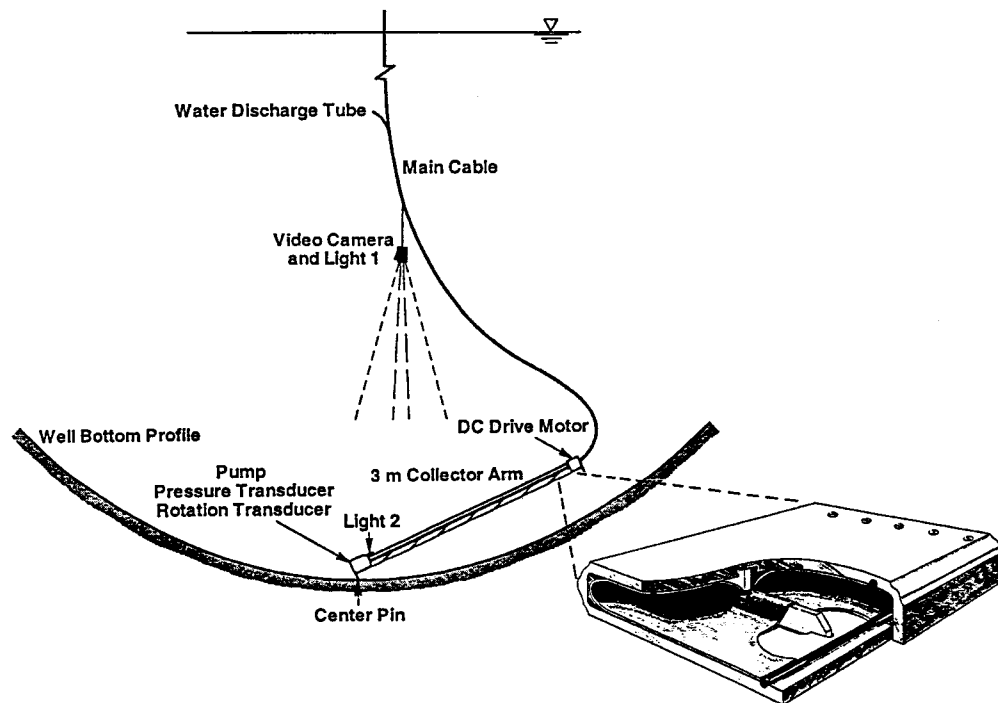


Figure 3. Original collector concept (layout and filter arm cross-section).

Particulate concentrations expected

We determined the filter mesh size and required area using information on the size distribution and amounts of particulates in Antarctic ice and estimates of extraterrestrial particle concentrations in Greenland and Antarctic ice.

The number of particulates in Antarctic ice <30 μm have been determined using Coulter counters (unpublished data from E.M. Thompson) and by counting the number of particles from photomicrographs taken using a scanning electron microscope (Higashi et al. 1990). The number of particles is very high: 20,000 particles/mL of water for sizes less than 1 μm , and about 7000 particles/mL of water in the 1–30- μm size range (unpublished data from E.M. Thompson). These particles are overwhelmingly terrestrial in origin. Thus, to avoid clogging our filter with terrestrial particles, we chose a filter fabric with a 53- μm opening. This should limit our collection to particles larger than about 50 μm unless the filter plugs significantly. These larger particles are easy to handle and analyze.

We estimated the fraction of extraterrestrial to terrestrial particles in Antarctic ice larger than 50 μm using data from Maurette et al. (1991). They melted 100 tons of Antarctic ice and recovered about 10 grams of particulate material. This material included 9000 micrometeorites 50 to 100 μm in diameter, 6500 micrometeorites 100 to 400 μm in diameter, and 9 micrometeorites larger than 400 μm . Assuming an average density of 2.5 g cm^{-3} , and taking 75 μm as the average diameter for the 50- to 100- μm -sized particles, 250 μm for the 100- to 400- μm particles, and 400 μm as the diameter

for particles larger than 400 μm , we estimate that 0.15 g of the 10 g recovered, or about 1.5%, was extraterrestrial.

Maurette et al. (1987) estimated the micrometeorite flux rate falling on Greenland ice as $6.3 \times 10^{-6} \text{ g m}^{-2} \text{ yr}^{-1}$ for the 50–300- μm size range. Love and Brownlee (1993) measured the micrometeorite flux rate in space, using the Long Duration Effects Facility, as $40 (\pm 20) \times 10^6 \text{ kg yr}^{-1}$, or 1.2×10^{-4} to $3.9 \times 10^{-5} \text{ g m}^{-2} \text{ yr}^{-1}$. The difference between the LDEF and the Greenland values suggests that 5 to 15% of the particles survive atmospheric passage. Figure 4 shows the size distribution of micrometeorites expected at the SPWW based on the Greenland flux rate. Our original estimate for the diameter of the SPWW was 15 m and that 10 m of downward melting (100 years of deposition) would occur each year. Thus, we expected that yearly collection could yield 0.11 grams of micrometeorites, or about 10^5 particles larger than 50 μm based on the flux rate of Maurette et al. (1987). However, we expected the first collection in 1995–96 to have three to four times this amount of material because of the larger ice volume melted to create and operate the well prior to our deployment.

We also expected the operation of the SPWW to add particulates to the well. To determine an approximate count, we asked John Rand to filter 8 L of water from the SPWW through a cellulose nitrate membrane filter with a 5- μm pore size. We examined the filter both optically and with a scanning electron microscope. Eleven percent of the surface area of the filter yielded 15 fibers and 568 particles, most in the 5–10- μm size range. Forty-

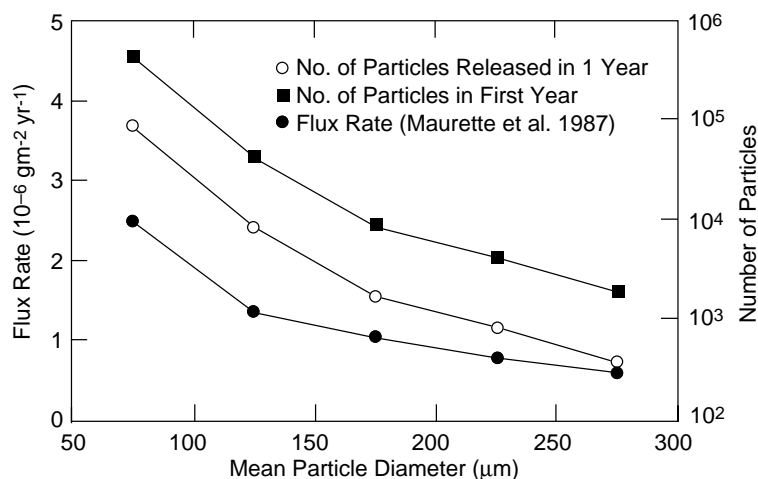


Figure 4. Number and size distribution of particles >50 μm estimated for the bottom of the SPWW.

four particles were larger than 50 μm . A random sampling of these particles using an SEM/EDX found a copper sulfate grain, an alumino silicate with some CuS on its surface, a fibrous particle (probably plastic) with some mineral fragments adhered, a very platy alumino silicate that contained Mg, Ca, and Fe, possibly a clay, several plastic pieces, and four particles containing Fe, Ni, Cr, Pb, Al, Si, and a trace of S. Most of these particles probably come from the heat exchanger, pump, and hoses used to operate the well. Assuming that the number of particles found in the 8-L sample is representative of what would be found in 2000 m^3 (the amount of water melted during one year of operation), that all these particles were from the well equipment, and that they settle to the bottom and are collected by our device, 10^8 terrestrial particles would be added to our collection, or about 1000 terrestrial particles for each extraterrestrial particle larger than 50 μm . Annual collection would thus yield a total of about 100 g of material.

The 8-L sample also revealed the presence of submicron particles of iron oxide in the well water. The white, cellulose nitrate membrane filter turned a bright orangish color after filtration, and energy-dispersive X-ray analyses of the filter showed only the presence of iron. The rust is thought to be from the heat exchangers or pump used for the well. Until January 1994, the water in the SPWW was acidic (pH 4.8), very soft,* and corrosive to metals. NSF has neutralized the water (pH 6.9) by running it through a limestone bed. This measure may diminish the formation of iron oxide. In addition, a fire retardant (Ansul dust, similar to baking soda) was used during the 1994 well fire. Particles of this fire retardant, soot, and melted insulation could also have reached the well pool, although most should have deposited along the well neck.

PUMPING REQUIREMENTS AND PRELIMINARY TESTS

Our collector design allowed for almost 1 m^2 of 30-cm-wide filter fabric inside a 3-m-long filter arm using a single fold of the filter to create a pouch. We obtained a polyester filter consisting of 53- μm mesh openings and 10^8 openings/ m^2 . Thus, 1 m^2 of this filter should trap the expected

10^8 particles before plugging. Design guidance suggested using a pressure drop of 34 kPa (5 lb in.⁻²) across the filter to determine pumping requirements. We expected that this loss would dominate all pumping losses.

We estimated the required pumping rate from the velocity needed to entrain 1-mm-diameter sand particles in water (ASCE 1975). The average velocity in the intake slot must exceed the particle fall velocity of about 10 cm/s to carry these particles into the filter. In addition, the friction velocity between the filter arm and the ice surface must exceed the threshold value to initiate particle movement of about 3 cm s^{-1} . This requires that the average flow exceed about 15 cm s^{-1} , if we assume that the gap between the filter arm and the ice surface is about 1 mm. Both conditions are met if the average velocity exceeds 30 cm s^{-1} in a 1-mm-wide intake slot (or 15 cm s^{-1} in a 2-mm-wide intake slot). We selected a compact, submersible pump that could deliver 1.6 L s^{-1} at 34 kPa or about 50 cm/s through a 1-mm-wide \times 3-m-long intake slot. Near zero pressure, the pump delivers about 3 L s^{-1} (100 cm/s through a 1-mm-wide \times 3-m-long intake slot).

We expected that the high-pressure drop through the filter and the narrow intake slot would establish relatively uniform intake velocities along the slot. Nevertheless, we conducted flow tests on a 30-cm-long \times 13-cm-wide model of the filter arm (front-slot version, Fig. 3) to verify particle pickup and assess the velocity distribution. This model contained pressure taps that allowed us to measure the pressure drop across the intake, the filter, and the plenum areas at three cross-sections along the collector. We also measured the total flow rate. For these tests, we prepared mixtures of simulated extraterrestrial particles consisting of stainless steel and glass spheres and silica sand, covering a size range of 50–420 μm .

We found no appreciable plugging of the filter (negligible increase in pressure drop across filter, negligible decrease in flow rate) even after collecting 68 g of material. The maximum pressure drop across the 53- μm filter was 4.2 kPa, and the corresponding minimum flow rate was 0.31 L s^{-1} (representing 100 cm s^{-1} through the 1-mm-wide \times 30-cm-long intake slot). The collector model easily suctioned up particles lying several millimeters in front of the intake. However, because the flow velocity drops quickly inside the collector, the collected particles were deposited on the bottom of the filter pouch downstream of the slot rather than evenly plugging the fabric.

*H. Mahar, 1996, National Science Foundation, personal communication.

These tests also revealed several disadvantages of our original, front-slot design: (a) filter installation was awkward, (b) it would be difficult to control the slot width if the arm was made from flexible plastic, and (c) the flow-collecting plenum channel downstream of the filter needed to be larger to reduce the pressure drop (and hence maintain a more uniform intake velocity distribution) along the collector arm.

For these reasons, we modified the collector-arm design to produce a central intake slot and a flow plenum channel along each side (Fig. 5). The arm can be fabricated from a machined and folded piece of low-density polyethylene (LDPE). O-rings secure the sides of the filter fabric adjacent to the intake slot, and folding results in a filter pouch. End caps with O-rings seal the filter pouch and prevent flow leakage. Aluminum ribs spaced along the arm maintain the geometry of the arm and slot and prevent collapse of the plastic under suction. Although this design draws flow equally from both directions under the collector, resulting in lower velocities along the ice surface, we felt the manufacturing, assembly, and flow-distribution advantages outweighed this disadvantage.

We conducted flow tests on a 30-cm-long \times 18-cm-wide model of the central-slot collector arm. This model developed better flow distribution, as evidenced by a lower pressure drop through the filter and negligible pressure drop along the plenum channels. It also easily suctioned up the test particles. No appreciable plugging of the filter occurred even though it collected almost 200 g of material, and the resulting minimum flow rate was 0.33 L s^{-1} . It was also much easier to install and remove filters with this model. With careful machining, a relatively uniform intake slot was

formed by folding and securing the two sides of the arm.

An important modification resulted from these tests. We found that particles could escape back through the intake slot when we pulled the collector out of the water and the pump lost suction. To prevent this “backflushing” of particles, we installed a thin strip of 1- μm filter fabric (later replaced with a strip of thin LDPE) to serve as a flow check valve. This solved the backflushing problem.

FINAL DESIGN

We constructed two fully operational collectors based on the central-slot design. We initially built a 1.2-m-long prototype to assess the design’s maneuverability and collection efficiency on iced surfaces. This prototype also provided us with a shorter, more maneuverable collector to use in the SPWW as an alternative to the 3-m-long device originally planned.

Figure 6 shows the basic features of the 1.2-m collector. The filter arm consists of a single machined and folded sheet of LDPE with the same internal layout as the 30-cm-long model (Fig. 5). This arm is quite flexible, allowing the collector to conform to a surface curvature of about 2 m radius (30 cm rise over 1.2 m). The LDPE also exhibits its low friction on wet ice. A central, waterproof aluminum housing contains the pump and drive motors and all electrical connections; the externally mounted pump housing is also aluminum. O-rings seal the removable end plates and motor shafts. Traction is via heavy, stainless steel, spiked wheels driven by DC gear motors through articulated alu-

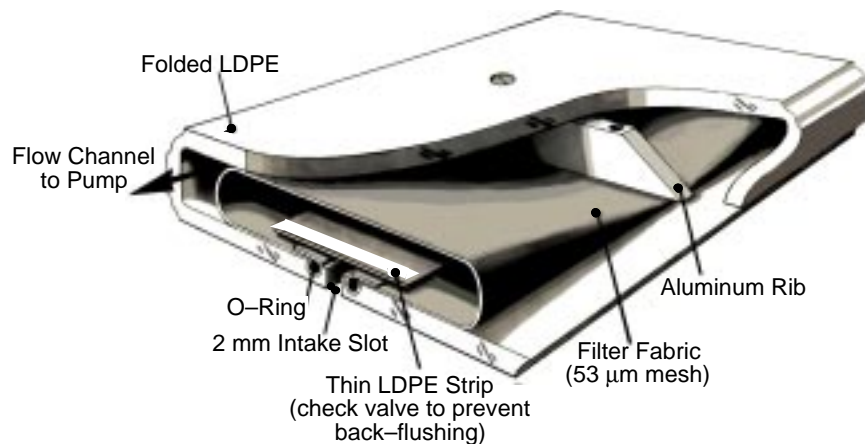


Figure 5. Final collector-arm cross-section.

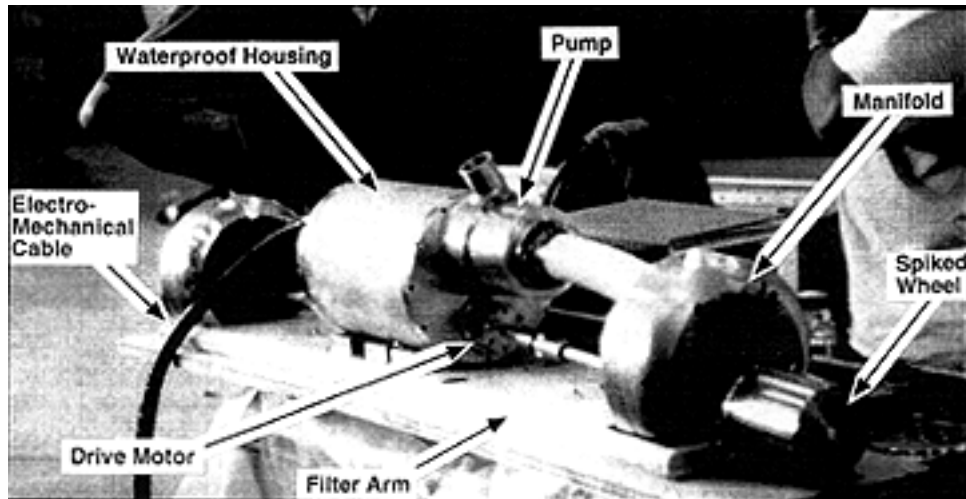


Figure 6. Major components of the 1.2-m operational collector.

minimum shafts. The manufacturer rated these motors for a continuous duty torque of 4.6 N-m. At each end of the arm, heavy aluminum assemblies guide the motor shafts and help the collector conform to surface curvature. In addition, one of these end assemblies contains an internal flow passage (manifold) to connect the pump to the two plenum chambers along the arm.

An electromechanical cable connects to the central housing via a waterproof connector. This custom-made, LDPE-jacketed cable contains 19 electrical conductors to operate the collector, underwater video camera, and lights at the SPWW. It also contains an internal Kevlar braided jacket, with a rated breaking strength of 4500 N, to act as a strength member. Mechanical attachments at the housing and end assembly transfer the weight of the collector to the cable. This 17-mm-diam. cable is quite flexible and can bend to a minimum radius of 30 cm at -50°C . All collector and cable components were accepted for use in the SPWW. Figure 7 shows a schematic of the 1.2-m collector, cable, camera, and lights in the SPWW.

We also constructed a 2.4-m-long, central-slot collector (Fig. 8). We chose this length for the filter arm because the longest sheet of LDPE available to us was 2.4 m. This collector utilizes similar components but is completely independent of the 1.2-m collector. It possesses two waterproof housings, each fitted with a pump and drive motor. Both aluminum end assemblies contain internal manifolds to connect the pumps to the plenum chambers in the arm. We can replace one drive wheel and motor with a 90° gear box and rotation transducer to measure the rotation of the arm around a pivot

point. The same electromechanical cable operates either collector. Many of the individual components are interchangeable between the 1.2-m and 2.4-m collectors, providing a level of redundancy; we also purchased numerous spare parts, including a second electromechanical cable.

The underwater video camera consisted of a high-resolution color camera and a zoom lens mounted inside an aluminum pressure housing (rated to 1000-m water depth). A thermostatically controlled heater ensured normal camera operation at -50°C . Two independently operated 500-W waterproof lamps provided illumination, with one projecting sideways from the collector and one projecting downward from the camera. Waterproof connectors connected the camera and lamps to the electromechanical cable. This equipment was operated through a video control unit and a video monitor at the surface.

The video system provides the visual feedback needed to maneuver the collector. We control the rotation speed and direction of drive motors using two DC power supplies at the surface. Current limiters ensure operation of the motors below their continuous-duty torque ratings. A simple rectifier and switch are sufficient to operate the collector pumps. We can monitor the current drawn by the pumps to determine the approximate flow rate.

A reversible, constant-speed winch raises and lowers the collector via the electromechanical cable. A set of slip rings provide electrical connections between the rotating cable and the stationary surface equipment. The cable passes over a 76-cm-diam. sheave mounted on top of a 3.6-m high

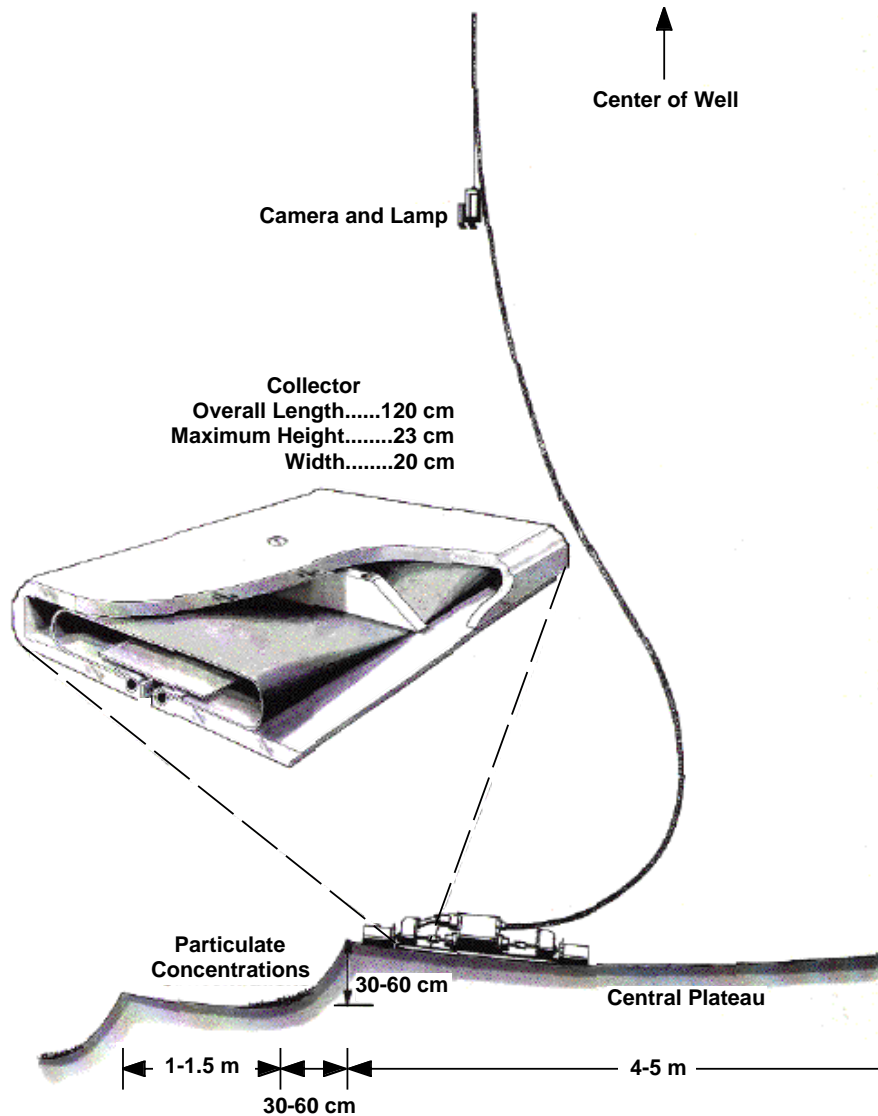


Figure 7. Schematic of the 1.2-m collector in the SPWW.

tower and then connects to the collector (Fig. 8). The tower allows the collector to hang vertically before descending through the well neck; it also allows the cable to warm slightly during ascent before bending over the sheave. The winch, tower assembly, and video and collector control equipment fit inside the winch room located directly above the second access hole to the SPWW (Fig. 2).

Prototype tests and modifications

Validating the performance of our particle collection system prior to its first use at the South Pole was an essential step in our design plan. We

arrived at the final collector designs through a series of laboratory tests, primarily using the 1.2-m collector prototype. The goals of these tests were to assess the collector's maneuverability and collection efficiency on submerged, iced surfaces and to make modifications as warranted before building the 2.4-m collector. We used two main test facilities: a 1.5 m × 1.5 m × 0.3-m-deep tank with a cold plate on its bottom to grow a flat layer of ice, and a 2.5-m-wide × 6-m-long × 3.6-m-high iced ramp with a curved parabolic profile that approximated published shapes for earlier Rodriguez wells (Schmitt and Rodriguez 1963, Russell 1965, Williams 1974, Lunardini and Rand 1995). We



Figure 8. 2.5-m operational collector suspended from the cable on a winch.

could submerge the iced ramp in a 9-m-wide \times 37-m-long \times 2.4-m-deep refrigerated basin. This provided the most realistic simulation of the collector's operation in the SPWW; however, we were unable to conduct quantitative collection-efficiency tests with this arrangement.

We quickly found that collector maneuverability was very good on both the flat and curved iced surfaces. The heavy spiked wheels provided excellent traction, and motor torque was adequate

for the collector to climb up the ramp to a location with a 45° downward slope. Pump suction did not affect collector mobility.

We conducted four quantitative collection efficiency tests, all using the 1.2-m collector in the 1.5-m iced tank. In all four cases, we used a 53- μ m polyester filter and a 5-cm-wide strip of LDPE as a check valve. We again used mixtures of stainless steel, glass spheres, and silica sand to simulate micrometeorites in a size range 60–400 μ m. We weighed the particulates added to the tank before testing and the particulates recovered from the collector filter after testing to determine the overall collection efficiency. Table 2 summarizes the results of these tests.

The ice surface formed on the cold plate was quite flat across the tank (with only 3- to 5-cm-wide strips of thinner ice along the tank walls) and generally very smooth (with only a few isolated depressions 1–2 mm deep and 1–2 cm wide, made as we added water to fill the tank). We tested the collector on this smooth ice during the first, and half of the second and third, collection-efficiency tests. For half of the second and third tests and all of the fourth test, we roughened the ice with a water jet to create numerous depressions 2–10 mm deep and 1–2 cm wide.

The collector suctioned test particles very well from smooth ice surfaces, collecting almost all the particles in a single pass. Particles remaining after the first pass were usually concentrated in the local depressions. Each additional pass would retrieve some particles from the depressions, but the collector would not generally clean them entirely. Nevertheless, the first three tests all yielded collection efficiencies over 99% (Table 2) despite the presence of intentionally roughened ice during half of the second and third tests. Interestingly, the collector achieved these high collection efficiencies despite leaving clearly visible patches of particles, mostly concentrated in the depressions but also in

Table 2. Summary of quantitative collection efficiency tests. All tests were conducted in 1.5-m iced tank.

Date	Material added (g)	Material recovered (g)	Percent recovered	Remarks
29 Jun	390.1	387	99.21	Smooth ice, multiple passes
30 Jun	100.1	99.54	99.44	Smooth ice surface 50 g, rough ice 50 g
6 Jul	100.0	99.46	99.46	Smooth ice surface 50 g, rough ice 50 g
10 Jul	231.51	206.38	89.15	Rough ice surface

lower concentrations on the flat ice. For example, the second test left only 0.6 g of the 100.1 g of particles added, yet particle patches were clearly visible.

The collector had much more difficulty collecting particles from the extensively roughened ice surface made for the fourth collection efficiency test. It achieved a collection efficiency of only about 89%. Some of the remaining particles, however, were frozen onto the bottoms of the depressions, suggesting that the test technique may have affected the recovery. Nevertheless, we did not know what the SPWW bottom roughness would be like, and we wanted to develop a method to retrieve particles easily from rough ice.

We made several minor modifications to the collector during the collection-efficiency tests based on the observed performance. The first test revealed that the flat-bottomed collector could press particles into very flat ice and be unable to collect them. We subsequently tested the collector with 1.5-mm-diam. Teflon-coated wires wrapped around the filter arm at the locations of the internal ribs. We tested these “runners” during the second and third tests and found that the collector did not press the particles into flat ice and it achieved good collection efficiency. However, the collector could retrieve particles better from deep depressions without these runners. We still brought a quantity of this wire to the SPWW for use if the well-bottom ice appeared to be very smooth (we did not use it).

We also developed (but again did not use in the SPWW) a method to retrieve particles from rough ice. This involved attaching an 8-cm-wide strip of thin LDPE (the same material used for the check valve) to the underside of the collector arm adjacent to the slot. This external flap would seal itself to the ice surface when the pump was on. Flow could only bypass the flap through deep depressions, effectively cleaning these depressions of particles, or by entering the slot from the other side of the collector, essentially doubling flow velocities. We tested this arrangement in a separate collection efficiency test on very rough ice. It picked up particles extremely well, even from 1-cm-deep depressions, and left the ice visibly clean after a single pass. Unfortunately, the shipping deadline prevented us from conducting a quantitative collection efficiency test, but the visual evidence from the test conducted suggests that it would have been greater than 99%.

We routinely measured flow rates through the 1.2-m collector during the collection efficiency

tests. The flow rate was consistently 2.1 L s^{-1} , independent of ice conditions, the presence of runners, and the amount of material collected (up to a maximum of 212 g preceding a flow measurement). Unlike the 30-cm-long model, however, it was difficult to achieve a uniform slot width along the 1.2-m-long prototype. For the first two collection efficiency tests, the slot width averaged about 1 mm, but varied between about 0.5 and 1.5 mm. This yielded an average gap velocity of about 170 cm s^{-1} , much higher than that needed for particle pickup. Because we were concerned that the narrow slot sections corresponded to areas of poor particle pickup, we attempted to machine the slot to a uniform width of 2 mm. We achieved an average slot width of 1.64 mm (Fig. 9), but local variations ranged from just under 1 mm to 2.8 mm. This yielded gap velocities that ranged from 64 to 190 cm/s and averaged 125 cm s^{-1} (assuming a uniformly distributed total flow of 2.1 L s^{-1}), well exceeding the target minimum of 10 cm/s . This velocity distribution did not appear to affect overall collection efficiency (the collector recovered over 99% of the particles deployed on combined smooth and rough ice during the third test), and we no longer saw any correlation between narrow slot width and poor particle pickup. We made no further changes to the slot prior to field deployment.

We also conducted particle-collection tests using the 1.2-m collector in the iced ramp, submerged in the refrigerated basin. Although these tests were qualitative, visual evidence indicated good collection efficiency where the collector contacted the surface. However, the collector left particle patches on the ramp in areas where it did not conform well to the surface shape. We therefore added weight inside the waterproof housing to allow the collector to conform to more severe surface curvature.

The modifications resulting from these tests on the 1.2-m collector were essentially options to improve collection efficiency on very smooth, rough, or curved ice and did not affect the basic design. Thus, we constructed the 2.4-m collector essentially as designed (see Appendix B for a summary of the collector development tests).

We tested the 2.4-m collector only on the iced, submerged ramp. The collector was quite maneuverable and could sweep across a region with a 45° upward slope. However, as with the 1.2-m collector, we added extra weight near the center of the collector to help it conform to the ramp and thereby improve its collection efficiency (documented visually). The spiked wheels could slip or cut through the ice at the steeper ascent angles, so

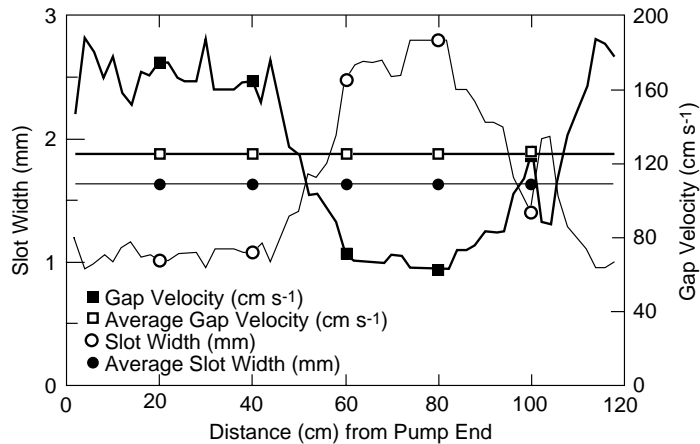


Figure 9. Slot width measured along the 1.2-m collector prior to deployment. Also shown is the corresponding gap velocity, assuming a uniform distribution of 2.1 L s^{-1} total flow.

to increase traction we manufactured longer drive shafts that could accept a double set of heavy, spiked wheels. These same long shafts and the spare wheels also fit the 1.2-m collector (optionally to increase its traction).

In addition to these tests on the assembled collectors, we cold-soaked individual components (silicone hoses, LDPE filter arm, O-rings, etc.) at -65°C in a liquid-nitrogen-cooled chamber (Tantillo 1993) to check their flexibility and durability. We also suspended each collector from our tower and sheave to ensure that they hung true.

Deployment

We sent two fully operational collectors to the South Pole with the means to make modifications to each should the well-bottom conditions be different from our expectations. We also shipped a winch, tower, and sheave, two 200-m electromechanical cables, a video camera, monitor, and recorder, spare pumps, filter fabric, and motors and various tools that we needed for assembly and repair of the collector in Antarctica. The operation of all these components was checked before shipping. The collectors and cables were disinfected using a 1:60 solution of Clorox® to water and were wrapped in plastic to stay clean during transit.

At the Pole, personnel from Antarctic Support Associates (ASA) assisted us in many ways. Their main task was to build the surface facilities that would provide us access to the SPWW and create an adjoining work space. They first dug a pit (about $3 \text{ m} \times 3 \text{ m} \times 3 \text{ m}$) in the snow adjacent to the existing wellhouse and down to the EPDM liner. We then cut a 30-cm square opening in the

liner, and ASA constructed and installed an EPDM-lined wooden chimney over the opening. We sealed the chimney to the opening. This process ensured continuity of the EPDM liner around our access hole and work area. ASA then carefully backfilled the pit with snow and constructed our work space. This work space consisted of a winch room directly over the chimney and an adjoining laboratory (Fig. 10).

We used a hot-water drill (Fig. 11) to make the second access hole to the SPWW; ASA also assisted with the drilling. Water from the well was heated in boilers located in the wellhouse and fed into the 30-cm-diam. cylindrical drill via a neoprene rubber hose. This hot water discharged through a 90° -cone nozzle to melt the ice as the drill descended. A water pump positioned inside the drill pumped water from down-hole to the surface via a return hose. The drill was lowered using a winch and stainless steel cable. The hoses were attached to the cable with stainless clamps and cloth ties. The cable was guided into the hole using a sheave suspended from a spring scale. The scale allowed us to determine whether the drill was suspended in air, was on ice, or was in water; this set the drilling rate. Drilling took about 36 hours, longer than expected, but yielded a vertical, wavy-walled access hole with a minimum clearance of 30 cm in diameter.

Prior to collector deployment, we lowered the video camera to examine the hole and inspect the well-bottom topography. We noticed that an ice cover had formed on the well pool and that the access hole through it had refrozen (we would need to break through this ice cover before each



Figure 10. Work space at the SPWW, consisting of a winch room directly over the access hole and an adjoining laboratory.

collector deployment). More importantly, the camera revealed that the well bottom contained isolated dark pockets of particulates and that these pockets coincided with sculptured features in the ice that were arcuate and half a meter deep. We decided to deploy the 1.2-m collector because it could more easily negotiate the sculpted topography than could the 2.4-m collector.

We successfully deployed and retrieved the 1.2-m collector six times and obtained five separate collections (one filter deployed twice) totaling about 200 g of material. Appendix C lists the deployments and shows the collector configuration for each. The collector provided a scale upon which to judge the well-bottom topography. It was much more complicated than we expected based on published shapes of earlier Rodriguez wells (Schmitt and Rodriguez 1963, Russell 1965, Williams 1974, Lunardini and Rand 1995). It consisted of a gently curved central plateau (about 18 m²) sculptured at its periphery into fairly steep arcuate dips that were 0.3–0.6 m below the plateau and 1–3 m wide; these dips led to smaller plateaus (1–3 m²) (Fig. 12). Farther away from the center, the bottom rose steeply and the sculptured features appeared to be more severe (either deeper or at



Figure 11. Hot-water drill used to drill second access hole to the SPWW.

shorter length scales). Associated with most sculptured features were dark pockets of particulates. Particles on the plateau areas were visible but not concentrated into pockets. Local surface roughness was quite smooth (perhaps 1-mm depressions over 1–5 mm scales). For this reason, we did not use the Teflon-wire runners or external LDPE flap (developed for very smooth or rough ice, respectively).

The collector maneuvered easily over the central plateau, and we devoted one collection (no. 3) exclusively to the plateau. Movement onto the adjoining dips and plateaus was possible with some practice, and we collected from five of these (about 10 m² total), including three particle pockets. We collected as much as 50 g of material at once without appreciably reducing pumping efficiency. Plateau areas suctioned were visibly clean, and gently curved dark areas changed from black to white with a single pass. This indicated high-efficiency particle pickup, based on our laboratory experience.

Good contact between the collector bottom and the ice surface was the most serious limit to collection efficiency in severely curved areas, and we maneuvered the collector slowly across the associated pockets to maintain good surface contact. This technique worked well but was very time-consuming. During some deployments, the field

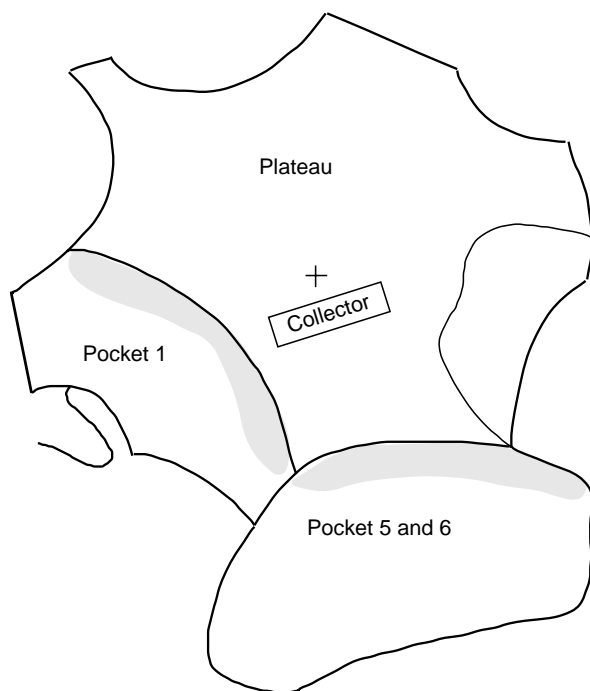


Figure 12. Map of the bottom of the SPWW showing the plateau area and pocket no. 1.

of view of the video camera limited our ability to maneuver the collector. We tried several techniques, unsuccessfully, to orient the camera to follow the collector.

The spiked wheels, often doubled on each end, provided extremely good traction on the ice. The allowable motor torque, rather than traction, generally limited collector maneuverability on steep sections, although collector stability was also a factor. We normally worked around these limitations quite successfully, and could have substantially increased the area suctioned within the performance capabilities of the 1.2-m collector. Unfortunately, after about two hours of maneuvering during a deployment, the drive motors failed. Post-deployment inspection revealed that shearing of gear teeth in each motor's gearbox caused the failures. This repeatedly occurred, despite readouts from the drive-motor power supplies that indicated operation at about half of the continuous-duty torque rating provided by the motor manufacturer. After all four motors had failed once (by deployment no. 4), we continued to run the collector by interchanging gears between gearboxes; this provided us with about two hours of operation before motor failure for deployments 5 and 6.

We had planned to dedicate deployment no. 4 to repeat suctioning of the central plateau. This would have allowed us to calculate in-situ collection efficiency. Unfortunately, one drive motor failed at the start of that deployment, and we only covered about one third of the central plateau. Upon retrieval of the collector, we found very little material in the filter bag and decided to reuse it for the next deployment to save time. Although not quantitative, the results of deployment no. 4 and the visually apparent cleaning of particles from the ice suggests a high in-situ collection efficiency.

SAMPLES

After each deployment except no. 4, we brought the collector to the laboratory space and removed the polyester filter from the filter arm. The white flexible fabric allowed us to see particles and easily remove them by backflushing the filter. We backflushed each of the two samples we processed into a large HDPE funnel, using well water that we pressurized in an HDPE hand sprayer. Each sample, one from a pocket, the other from the plateau, was then wet-sieved into stainless steel sieves

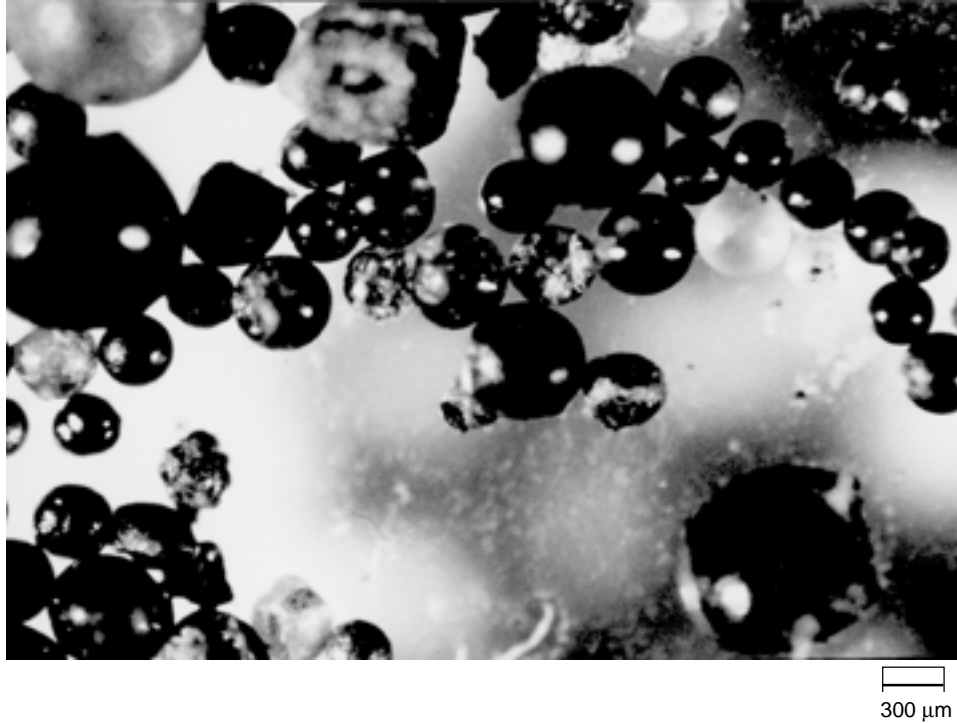


Figure 13. An assortment of spherules from the SPWW. The large sphere in the upper left corner is a copper contaminant ($\times 40$).

yielding 50–106- μm , 106–250- μm , 250–425- μm , and >425- μm size fractions. Using a binocular microscope, spheres were separated from these two samples by hand picking (Fig. 13). These two samples were processed in the field to assess the collector's performance and to determine the type and amount of materials recovered. The remaining three samples were placed in bags, sealed, and shipped to CRREL for later analysis.

Other than well water, no solvents were used in the separation process. We collected aliquots of everything the particles may have come in contact with (drilling water, water, and residue left after backflushing and sieving a collection). We also exposed a section of clean filter to the wellhouse environment, as suggested by Michael Zolensky. These samples can be analyzed if any unexpected contaminants are found in the particles.

About 200 g of material were recovered from the well bottom. Most of the material was terrestrial (Fig. 14), predominantly rust grains injected into the well and originating either from the heat exchanger or from the non-stainless steel components within the pump. There were also wood fragments, paint chips, wire, and aluminum flakes.

Our initial examination of the collected sedi-

ment focused predominantly on spherical particles. Although not all spherical particles are extraterrestrial (there were copper spheres formed when pipes were soldered and dark, nonmagnetic "glue balls" thought to have formed during the fire), spheres can be rapidly separated with an ordinary binocular microscope. Those that are "cosmic" can then be separated by their several unique properties. Previous studies have shown that cosmic spherules have distinctive mineralogy, bulk chemistry, internal and surface textures, and are usually moderately magnetic (Brownlee 1981). Here we used their abundance as a measure of the amount of extraterrestrial material in our samples.

All 6.01 g of the 250–425- μm size fraction of pocket collection no. 1 and all 3.5 g of the 250–425- μm size fraction of the plateau collection were examined. Table 3 lists the number of cosmic spherules found in these two fractions. Assuming an average particle weight of 3.5×10^{-5} g/particle (300 μm diam., 2.5 g cm^{-3}) gives a weight of 7.9×10^{-3} g for the pocket collection and 4.4×10^{-3} g for the plateau collection, or about one part per thousand melted meteoritic material. In addition to the 250–425- μm size fractions, 0.56 g of the 23.8 g of the 106–250 μm and 0.15 g of the 12.67 g of the 53–106 μm were also examined for the pocket collec-



Figure 14. 'Sediment' retrieved from the well ($\times 10$).

Table 3. Size range and weight of the pocket and plateau samples.

Size range (μm)	Pocket			Plateau		
	Weight (g)	No. of cosmic spherules	Flux ($\text{g m}^2 \text{yr}^{-1}$)	Weight (g)	No. of cosmic spherules	Flux ($\text{g m}^2 \text{yr}^{-1}$)
>425	6.4			5.4		
250–425	6.0	224	7×10^{-6}	3.5	126	6×10^{-7}
106–250	23.8			5.1		
53–106	12.7			2.9		
Total	48.9			16.9		
Area covered	5 m^2			17 m^2		

tion. If the subsamples are representative of the entire size fraction, then there are $2 \times 10^{-3} \text{ g g}^{-1}$ of material in the 106–250- μm size fraction.

The types of cosmic spherules found in the SPWW were assessed by mounting particles from the 250–425- μm and 106–250- μm size fraction in epoxy, sectioning them, and examining them using the Cameca SX-50 electron microprobe at the University of Tennessee, Knoxville. We found the full range of cosmic spherule morphologies (Table 4).

Photomicrographs of SPWW particles are presented in Figure 15a–h. *Glass spherules* are composed of mafic glass and represent particles that have been fully melted, devolatilized, and rapidly quenched during atmospheric entry (Fig. 15a). *Cryptocrystalline spherules* are predominantly glassy particles with crystallites too small to be individually recognized, surrounded by an iron-rich glass (Fig. 15b). *Barred olivine spherules* are particles that have also been fully melted but that were less rapidly quenched, allowing olivine and magnetite crystallites to form (Fig. 15c). *Relic-grain-bearing spherules* are particles that did not fully melt before quenching and retain “meteoritic” minerals, surrounded by an iron-rich glassy rim (Fig. 15d). *Volatile-rich spherules* are vesiculated particles showing regular to irregular cavities and lots of relic olivine, metal, or sulfide grains; they represent particles quenched quickly after initial heating, before full devolatilization could occur (Fig. 15e). The *G-type* are high-iron spherules and contain magnetite dendrites in a glass matrix (Fig. 15f). *Iron spherules* (I-type) are wholly metallic (Fig. 15g) and show meteoritic siderophile concentrations. *Unmelted* IDP-like particles have compact, irregular texture, with iron-rich rims around dispersed voids and relic olivine grains (Fig. 15h).

When compared to the other large collections

Table 4. Types of extraterrestrial particles in the pocket sample, 106–425 μm .

Glass	14
Cryptocrystalline	11
Barred olivine	51
Relic grain-bearing	7
Volatile-rich	3
High iron (G-type)	1
Iron	1
IDP-like	1
Total	88

of cosmic spherules—the Deep Sea spheres (Brownlee 1979) and the Greenland spherules (Maurette et al. 1987)—the SPWW materials are most similar to particles collected in Greenland (Table 5). The main difference is the higher proportion of glassy spheres and the lower percentage of unmelted materials in the SPWW collection. However, the fraction of unmelted micrometeorites in the SPWW will increase as we systematically look for them. The major differences between the SPWW spherules and those found in deep-sea sediments are the increase in glass spherules found and the paucity of iron and G-type spherules. This is true both for magnetically and nonmagnetically collected deep-sea spheres (Taylor and Brownlee 1991).

Twenty spherules from the pocket sample were analyzed using a Zeiss DSM962 at Dartmouth College. When plotted on a MgO, SiO₂, and FeO ternary diagram (Fig. 16) or on a Ca/Si vs. Al/Si plot (Fig. 17), the SPWW spherules lie within the field found for other collections.

Although detailed examinations of nonspherical particles have not yet taken place, the presence of one relatively large, unmelted particle in one of our mounts suggests a significant unmelted ET component. Unmelted particles have been found by previous studies of particles retrieved from melted Antarctic snow and ice. Further studies will incorporate a detailed examination of the nonspherical particles in the sediment.

Weathering

The barred olivine spherules show various degrees of weathering with preferential removal of Fe-rich glass interstitial to Mg-rich olivine bars. Some stony spherules retain a glassy rim (Fig. 18), while others show 10–20- μm grooves at their margins and occasionally significant removal of glass in their interiors. The one G-type spherule has a highly weathered core (Fig. 15f), and the iron spherule has lost the interstitial nickel-rich phase near its periphery (Fig. 15g). The weathering is probably caused by the acidic water in which the particles were immersed for up to 4 years. How weathering has affected unmelted particles is not yet known.

Flux rates

A terrestrial flux rate for meteoritic material 50–300 μm was obtained from Greenland ice (Maurette et al. 1987). To make this flux calculation, Maurette and his colleagues estimated the concentration of sediment in mature cryoconite

Figure 15. Backscattered electron photomicrographs of selected SPWW micrometeorites that include: a) a glassy spherule showing a bright network of convection borders; b) a cryptocrystalline to fine-grained spherule; c) a barred olivine spherule; d) a spherule containing several relic grains and small distributed FeNi patches; e) a volatile-rich spherule showing large irregular internal cavities; f) a G-type spherule containing magnetite dendrites in iron-rich glass; g) a metallic FeNi particle showing small ameoboidal domains and meteoritic composition; h) an IDP-like particle showing a Mg-rich phyllosilicate matrix, distributed relic FeNi metal and sulfide grains, and Fe staining at the rim and surrounding interior voids.

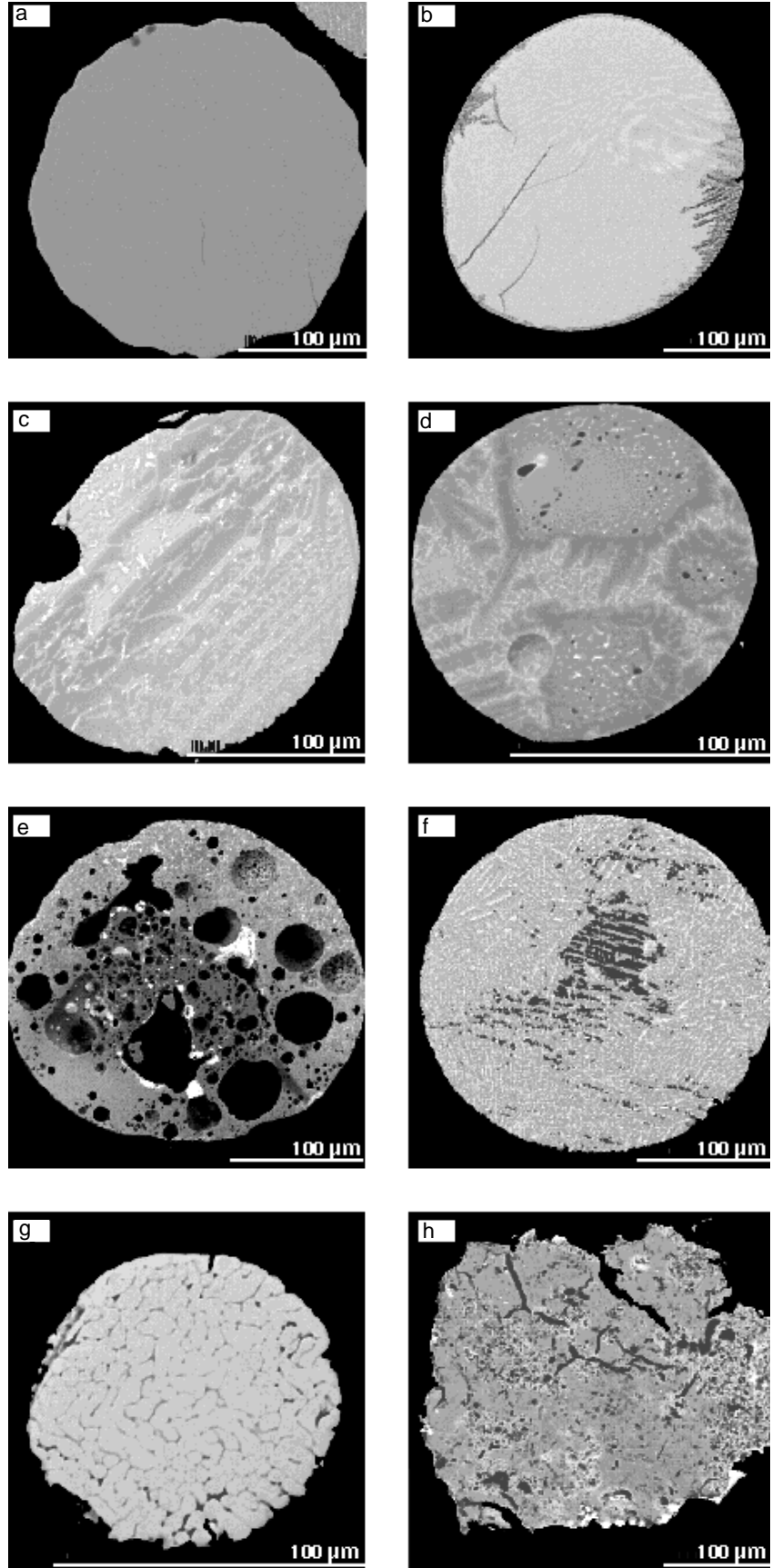


Table 5. Comparison of SPWW spherule types with those found in Greenland and in the Deep Sea collection.

	No. of spheres examined	Unmelted	Relic grains	Glass	Crypto- crystalline	Barred olivine	G-type	Iron
SPWW	88	5	8	16	12	57	1	1
Greenland	92	18	10	5	9	55	1	1
Deep Sea spheres (magnetically collected)	778	5	9	1	2	52	5	26
Deep Sea spheres (nonmagnetically collected)	146	6	10	1	5	44	7	27

Figure 16. Ternary diagram illustrating where the analyzed SPWW spherules plot in relation to the Deep Sea and Greenland spherules.

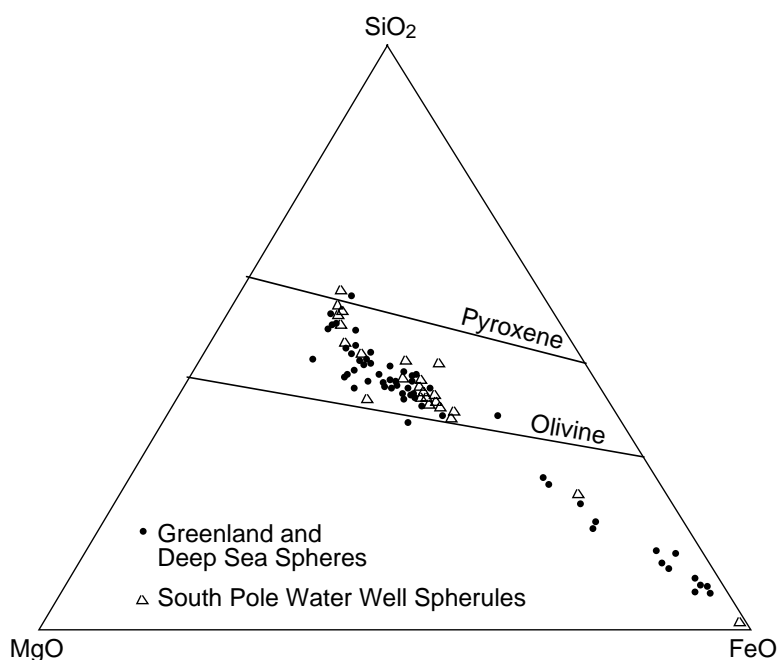
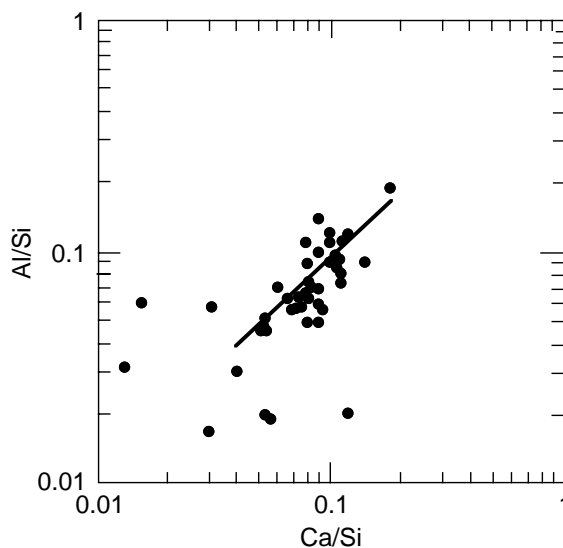


Figure 17. Weight percent Al/Si and Ca/Al plot of the SPWW spherules as compared to DSS and chondritic value.



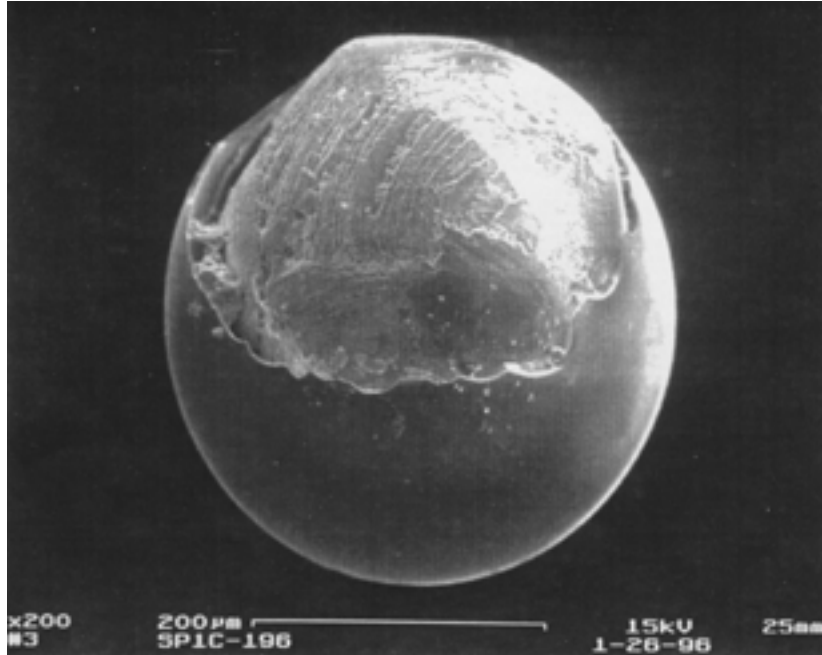


Figure 18. Photomicrograph showing a glass rind around a stony spherule.

deposits on the ice surface, estimated the age of the ice melted to form the deposits using an ice flow model, and assumed that all particles deposited had been collected. We have calculated a terrestrial flux rate for melted micrometeorites larger than $250\ \mu\text{m}$ for the pocket ($7 \times 10^{-6}\ \text{g m}^{-2}\ \text{yr}^{-1}$) and the plateau ($6 \times 10^{-7}\ \text{g m}^{-2}\ \text{yr}^{-1}$) collections; the latter is the same value found by Maurette et al. (1987) for their 250–300- μm size fraction. We know the volume of firn and ice melted to 10% and the age of the ice to 50 years (the uncertainty is due to the topography at the bottom of the well), and the area cleaned was determined from the video. Since we collected from 7% of the well bottom, the accuracy of our flux measurement will depend on the movement of particles along the bottom.

From the video footage we estimate that we collected from an area of $30\ \text{m}^2$, or about 7% of the well bottom. The pockets preferentially contain iron-oxide grains derived from the water-supply system; the circulating flow can easily concentrate this injected material. The order-of-magnitude-larger flux estimate for the pocket as compared with the plateau, however, suggests that the well circulation is also concentrating micrometeorites into the pockets. This is despite the relatively small flow rate (about $1\ \text{L s}^{-1}$) discharged about 13 m

above the bottom and no trace of particle transport even with the collector nearby to act as a local disturbance. Perhaps the compressed air entrapped in the ice releases bubbles into the water as the well melts downward, and this agitation helps to entrain the micrometeorites.

It is not clear whether or not the particles are being removed from the plateau into the pockets; the micrometeorites in the pockets may come from the well sides. If micrometeorites are not being moved from the plateau area, repeat collections of the plateau could provide information on flux rates and on any temporal changes in the type and number of micrometeorites. Detailed analysis of the separate collections from the central plateau and the isolated pockets will reveal the degree of micrometeorite concentration possible by the circulating flow.

CONCLUSION

We have successfully recovered extraterrestrial materials from a polar well. This is thought to be one of the largest and best preserved collection of micrometeorites, and it is the best dated. This collection will allow us to calculate flux measurements of cosmic dust larger than $50\ \mu\text{m}$ and will

give us an understanding of the breadth of materials present in the solar system in this size range.

Our collector worked well despite the severe well topography. We learned that a 2.5-m collector is too long and is not needed for the conditions we encountered; that available motor torque (rather than traction) limited the collector's mobility over the well bottom; and that visual feedback is essential to negotiate the well's complex topography (our camera lacked the ability to track the collector more than 5 m away from the center). We hope to install more powerful motors and a pan/tilt camera to overcome these problems and thus to increase the collection area and operational efficiency. However, the more severe topography away from the center of the well dictates the need for a second, smaller, and more agile collector.

The complex bottom topography in the SPWW precluded our suctioning the entire bottom. We suctioned a gently curved, central plateau (about 18 m²) and three surrounding pockets (about 12 m² total) and should be able to return to these areas annually to determine flux rates. From the five collections, we retrieved approximately 200 g of material. Microscopic examination of the 250 to 425- μ m size fraction from two of the five collections suggests that one of every 1000 particles in this size fraction is a melted micrometeorite. Not counted are the unmelted micrometeorites present. We think the flux value for the plateau of 6×10^{-7} g m⁻² yr⁻¹ is a minimum. The circulation velocities seem too low to add particles to the plateau, and we did not include unmelted particles in this estimate. With unmelted micrometeorites included, the flux rate we calculate for the SPWW will be higher than that found by Maurette et al. (1987) in Greenland.

The particles retrieved will be analyzed and compared with other cosmic dust collections to determine differences in composition and weathering patterns. Because of the large number of particles recovered, it is likely that very large IDP-like micrometeorites, extremely rare in other collections, will be found. In addition, identification of the terrestrial components (pollen, diatoms, ash, etc.) from these samples would allow a statistically significant study of circum-Antarctic wind circulation during these time periods.

LITERATURE CITED

- ASCE (1975) *Sedimentation Engineering*. ASCE Manuals and Reports on Engineering Practice No. 54. New York: American Society of Civil Engineers.
- Blanchard, M.B., D.E. Brownlee, T.E. Bunch, P.W. Hodge, and F.T. Kyte (1978) Meteor Ablation Spheres from Deep-Sea Sediments, NASA Technical Memorandum 78510.
- Bradley, J.P., S.A. Sandford, and R.M. Walker (1989) *Interplanetary Dust Particles, in Meteorites and the Early Solar System* (Kerridge and Matthews, Ed.). Tucson, Arizona: University of Arizona Press.
- Brownlee, D.E. (1979) Meteorite mining on the ocean floor (abstract). *Lunar Planet. Science*, **10**: 157–158.
- Brownlee, D.E. (1981) Extraterrestrial components. In *The Sea 7* (C. Emiliani, Ed.). New York: J. Wiley and Sons, Inc., p. 733–762.
- Brownlee, D.E., D.A. Tomandl, and E. Olszewski (1977) Interplanetary dust; a new source of extraterrestrial material for laboratory studies. In *Proceedings of the 8th Lunar and Planetary Science Conference, Houston, Texas*, p. 149–160.
- Brownlee, D.E., D.J. Joswiak, S.G. Love, A.O. Nier, D.J. Schlutter, and J.P. Bradley (1993) Identification of cometary and asteroidal particles in stratospheric IDP collections (abstract). In *Proceedings of the 24th Lunar and Planetary Science Conference*. Houston: Lunar and Planetary Institute, p. 205–206.
- Clark, E.F. (1965) Camp Century—Evolution of concept and history of design, construction and performance. USA Cold Regions Research and Engineering Laboratory, Technical Report 174.
- Czajkowski, J., P. Englert, Z.A. Bosellini, and J.G. Ogg (1983) Cobalt enriched hardgrounds—New sources of ancient extraterrestrial materials. *Meteoritics*, **18**: 286–287.
- Fredriksson, K., and R. Gowdy (1963) Meteoritic debris from the Southern California desert. *Geochimica et Cosmochimica Acta*, **27**: 241–243.
- Ganapathy, R., D.E. Brownlee, and P.W. Hodge (1978) Silicate spherules from deep sea sediments: Confirmation of extraterrestrial origin. *Science*, **201**: 1119–1121.
- Hagen, E.H. (1988) Geochemical studies of Neogene till in the Transantarctic Mountains: Evidence for an extraterrestrial component. M.S. thesis, The Ohio State University.

- Hagen, E.H., G. Faure, and C. Koeberl** (1992) Geochemistry of silicate spherules from till and ice cores in Antarctica: Evidence for anthropogenic spherules (abstract). *GSA Abstracts with Programs 1992*, a135.
- Harvey, R.P., and M. Maurette** (1991) The origin and significance of cosmic dust from the Walcott Névé, Antarctica. In *Proceedings of the 22nd Lunar and Planetary Science Conference, Houston, Texas*. Houston: Lunar and Planetary Institute, **21**: 569–578.
- Higashi, A., Y. Fujii, S. Takamatsu, and R. Watanabe** (1990) SEM observations of micro-particles in Antarctic ice cores. *Bulletin of Glacier Research*, **8**: 31–53.
- Jehanno, C., D. Boclet, Ph. Bonte, A. Castellarin, and R. Rocchia** (1988) Identification of two populations of extraterrestrial particles in a Jurassic hardground of the Southern Alps. In *Proceedings of the 19th Lunar and Planetary Science Conference, Houston, Texas*. Houston: Lunar and Planetary Institute, **18**: 623–630.
- Koeberl, C., and E.H. Hagen** (1989) Extraterrestrial spherules in glacial sediment from the Transantarctic Mountains, Antarctica; structure, mineralogy, and chemical composition. *Geochimica et Cosmochimica Acta*, **53**: 937–944.
- Krinov, E.L.** (1959) Über die Natur der Mikrometeoriten. *Chem. Erde*, **20**: 28–35.
- Kuivinen, K.C., B.R. Koci, G.W. Holdsworth, and A.J. Gow** (1982) South Pole ice core drilling, 1981–1982. *Antarctic Journal of the United States* XVII, p. 89–91.
- Langway, C.C.** (1963) Sampling for extra-terrestrial dust on the Greenland Ice Sheet, Union Géodésique et Géophysique Internationale, Association Internationale d'Hydrologie Scientifique. Berkeley Symposium, Pub. No. 61, p. 189–197.
- Love, S.G., and D.E. Brownlee** (1993) A direct measurement of the terrestrial mass accretion rate of cosmic dust. *Science*, **262**: 550–553.
- Lunardini, V., and J. Rand** (1995) Thermal design of an Antarctic water well. USA Cold Regions Research and Engineering Laboratory, Special Report 95-10.
- Marvin, U.B., and M.T. Einaudi** (1967) Black, magnetic spherules from Pleistocene and recent beach sands. *Geochimica et Cosmochimica Acta*, **31**: 1871–1884.
- Maurette, M., C. Hammer, D.E. Brownlee, N. Reeh, and H.H. Thomsen** (1986) Placers of cosmic dust in the blue ice lakes of Greenland. *Science*, **233**: 869–872.
- Maurette, M., C. Jehanno, E. Robin, and C. Hammer** (1987) Characteristics and mass distribution of extraterrestrial dust from the Greenland ice cap. *Nature*, **328**: 699–702.
- Maurette, M., C. Olinger, M. Christophe, G. Kurat, M. Pourchet, F. Brandstatter, and M. Bourot-Denise** (1991) A collection of diverse micrometeorites recovered from 100 tonnes of Antarctic blue ice. *Nature*, **351**: 44.
- McCorkell, R.H., W.H. Pinson, E.L. Fireman, and C.C. Langway, Jr.** (1970) A search for cosmic dust in a large collection of particulate and dissolved material from polar ice. *International Association of Science Hydrology*, **86**: 25–30.
- Murray, J., and A.F. Renard** (1876) On the microscopic characters of volcanic ashes and cosmic dust, and their distribution in deep-sea deposits. In *Proceedings of the Royal Society of Edinburgh*, XII, p. 474–495.
- Robin, E., M. Christophe, M. Bourot-Denise, and C. Jehanno** (1990) Crystalline micrometeorites from Greenland blue lakes: Their chemical composition, mineralogy and possible origin. *Earth and Planetary Science Letters*, **97**: 162–176.
- Russell, F.L.** (1965) Water production in a polar ice cap by utilization of waste engine heat. USA Cold Regions Research and Engineering Laboratory, Technical Report 168.
- Schmitt, R.P., and R. Rodriguez** (1960) Glacier water supply system. *The Military Engineer*, p. 382–383.
- Schmitt, R.P., and R. Rodriguez** (1963) Glacier water supply and sewage disposal systems. In *Symposium on Antarctic Logistics*, Boulder, Colorado, 1962. National Academy of Sciences, National Research Council, p. 329–338.
- Tantillo, T.** (1993) Design of liquid nitrogen temperature control system. USA Cold Regions Research and Engineering Laboratory, internal report.
- Taylor, S., and D.E. Brownlee** (1991) Cosmic spherules in the geologic record. *Meteoritics*, **26**: 203–211.
- Williams, J.S.** (1974) Experimental development of potable water supply for new South Pole Station. Technical Note N-1328. Port Hueneme, California: Civil Engineering Laboratory, Naval Construction Battalion Center.
- Yiou, F., and G.M. Raisbeck** (1990) Cosmic spherules from Antarctic ice cores as proxy indicators of extraterrestrial matter influx during the last 150,000 years. In *Workshop on Differences between Antarctic and non-Antarctic Meteorites*, LPI Technical Report 90-01. Houston: Lunar and Planetary Institute, p. 99–100.

APPENDIX A: SPWW DIMENSIONS

Table A1 contains measured well dimensions from the SPWW log book and measured water consumption from weekly South Pole situation reports (sitreps). Bottom depth (D) is the distance from the wellhouse floor to the bottom of the well; water level (L) is the distance from the wellhouse floor to the top of the water pool; pool depth (H) is the difference between bottom depth and water level ($H = D - L$); dQ/dt is the water volume consumed from the well during the one-week reporting interval; and Q is the cumulative volume of water consumed during the life of the well. Figure A1 plots these data as functions of time. Interestingly, the dimensions vary nearly linearly with time shortly after initial startup and after the restart necessitated by the 1994 fire. Note that freezing of the pool caused a 4-m-thick ice cover to form between 82.6–86.6 m depth.

Several “draw-down” tests were conducted during the history of the well to determine its radius (R): a known volume of water was withdrawn from the well and the drop in water level was measured. However, after consumption began, withdrawals of about 5 m³ would only yield water-level drops of about 1 ± 0.5 cm, producing large uncertainty in the estimated pool radii. Indeed, the 14 draw-down tests conducted in March/April 1995 yielded an average radius of 13.1 m with a standard deviation of 2.4 m. However, because dQ/dt was recorded from the onset of consumption, we may use these data in a water-balance formula to compute pool radius.

Figure A2 shows a schematic of the well pool and the resulting changes in dimensions as the pool deepens. The pool volume, initially V_p , increases to $V_p + dV_p$. This melts additional ice volume,

$$dV_i = dV_p + \pi R^2 dL, \quad (\text{A1})$$

so the incremental water created is

$$dV_w = \gamma_p dV_i = \gamma_p (dV_p + \pi R^2 dL), \quad (\text{A2})$$

where γ_p is the average ice specific gravity along the pool walls. The increase in pool volume then equals this increase in water created less any water volume consumed. That is,

$$dV_p = \gamma_p (dV_p + \pi R^2 dL) - dQ. \quad (\text{A3})$$

Rearranging eq A3 yields an expression for water consumption in terms of changes in pool volume:

$$dQ = \gamma_p \pi R^2 dL - (1 - \gamma_p) dV_p. \quad (\text{A4})$$

To use eq A4, we must assume an average shape for the pool. Lunardini and Rand (1995) assumed that the well would develop a paraboloid-shaped pool. However, shape data for previous Rodriguez wells (Rodriguez 1963, Russell 1965, Williams 1974, Lunardini and Rand 1995) and observed geometry from our 1995 deployments in the SPWW suggest that an ellipsoidal pool shape would also be a good approximation. For either case,

$$V_p = \alpha R^2 H \quad \text{where} \quad \begin{array}{ll} \alpha = \frac{\pi}{2} & \text{for a paraboloid} \\ \alpha = \frac{2\pi}{3} & \text{for an ellipsoid} \end{array} \quad (\text{A5})$$

Table A1. SPWW dimensions and water consumption from startup to the end of 1995 collector deployments.

	<i>Date</i>	<i>Comments</i>	<i>Bottom depth (m)</i>	<i>Water level (m)</i>	<i>Pool depth (m)</i>	<i>dQ/dt (m³/week)</i>	<i>Q (m³)</i>	<i>Estimated radius (m)</i>
1	12/8/92	startup		54.3				
2	12/9/92		64.3	59.5	4.9			3.4
3	12/10/92	meas. D=2.7 m	67.1	61.2	5.9			4.1
4	12/11/92	meas. D=3.1 m	68.9	62.3	6.6			4.6
5	12/12/92	meas. D=3.2 m	69.7	62.9	6.8			4.8
6	12/19/92		74.1	65.7	8.4			5.9
7	12/26/92		77.0	67.6	9.4			6.6
8	1/29/93		83.8	73.4	10.3			7.2
9	2/1/93		84.1	73.8	10.3			7.2
10	2/13/93			74.8				
11	3/14/93		87.5	76.5	11.0			7.7
12	4/10/93		89.3	78.3	11.0			7.7
13	4/24/93		89.9	79.0	11.0			7.7
14	5/1/93		90.2	79.0	11.3			7.9
15	5/8/93		90.5	79.0	11.6			8.1
16	5/15/93		90.9	79.3	11.6			8.1
17	5/22/93		91.2	79.6	11.6			8.1
18	5/29/93		91.5	79.6	11.9			8.3
19	6/5/93		91.8	80.2	11.6			8.1
20	6/12/93		92.4	80.5	11.9			8.3
21	6/19/93		92.5	80.5	12.0			8.4
22	6/26/93		93.0	80.8	12.2			8.5
23	7/3/93		93.3	80.8	12.5			8.8
24	7/10/93		93.9	81.3	12.7			8.9
25	7/17/93		94.2	81.4	12.8			9.0
26	7/24/93		94.4	81.6	12.8			9.0
27	7/31/93		94.8	82.0	12.8			9.0
28	8/7/93		95.1	82.0	13.1			9.2
29	8/14/93		95.4	82.2	13.3			9.3
30	8/21/93		95.6	82.2	13.4			9.4
31	8/28/93		96.2	82.3	13.9			9.7
32	9/4/93		96.6	82.6	14.0			9.8
33	9/4/93		96.6	82.6	14.0			9.8
34	9/11/93		96.6	82.3	14.3			10.0
35	9/18/93		97.0	82.3	14.6			10.2
36	9/25/93		97.3	82.6	14.6			10.2
37	10/3/93		97.4	82.9	14.5			10.1
38	10/9/93		97.6	83.1	14.5			10.1
39	10/16/93		97.6	83.1	14.5			10.1
40	10/23/93		98.2	83.2	14.9			10.5
41	11/3/93		98.3	83.4	14.9			10.5
42	11/6/93		98.6	83.7	14.9			10.5
43	11/13/93		98.8	83.8	14.9			10.5
44	11/20/93		98.9	84.0	14.9			10.5
45	11/27/93		99.1	84.1	14.9			10.5
46	12/4/93		99.2	84.1	15.1			10.6
47	12/11/93		99.4	84.1	15.2			10.7
48	12/18/93		99.5	84.3	15.2			10.7
49	12/25/93		99.5	84.3	15.2			10.7
50	1/1/94		99.8	84.5	15.4			10.8
51	1/8/94		100.0	84.6	15.4			10.8
52	1/15/94		100.2	84.8	15.4			10.8
53	1/22/94		100.3	84.9	15.4			10.8
54	1/29/94		100.5	84.9	15.5			10.9
55	2/4/94		100.6	85.1	15.5			10.9
56	2/12/94		100.8	85.2	15.5			10.9
57	2/19/94		100.9	85.2	15.7			11.0
58	2/26/94		101.2	85.4	15.9			11.1
59	3/1/94	fire-shut down						
60								
61								
62	11/26/94	repair ongoing						
63	11/30/94	shelf to 86.6 m	90.2	82.6	7.6			0.2
64	12/2/94	restart well	90.2					

Table A1 (Cont'd).

	<i>Date</i>	<i>Comments</i>	<i>Bottom depth (m)</i>	<i>Water level (m)</i>	<i>Pool depth (m)</i>	<i>dQ/dt (m³/week)</i>	<i>Q (m³)</i>	<i>Estimated radius (m)</i>
65	12/3/94		90.2	83.5	6.7			4.7
66	12/3/94			83.4				
67	12/4/94			83.4				
68	12/6/94			83.6				
69	12/7/94			83.8				
70	12/11/94		98.6	83.7	14.8			10.4
71	12/16/94		98.8	84.5	14.2			9.9
72	12/24/94		99.0	84.6	14.4			10.1
73	12/31/94		99.5	84.8	14.8			10.3
74	1/4/95		99.7	85.0	14.7			10.3
75	1/7/95	water samples	99.8	85.0	14.7			10.3
76	1/14/95		100.0	85.1	14.8			10.4
77	1/21/95		100.2	85.2	14.9			10.5
78	1/28/95		100.3	85.2	15.1			10.6
79	1/30/95	start consumption	100.5				0.000	10.7
80	2/2/95		100.7	85.5	15.2	32.32	32.320	10.7
81	2/11/95		100.9	85.6	15.3	43.24	75.560	10.7
82	2/18/95		101.4	85.8	15.6	27.30	102.86	10.8
83	2/22/95	pump failed						
84	2/25/95	pump replaced				23.33	126.20	
85	3/4/95		101.4	85.9	15.5	4.98	131.18	10.9
86	3/11/95		101.5	86.0	15.5	25.47	156.65	10.9
87	3/18/95		101.6	86.1	15.5	24.82	181.48	10.9
88	3/24/95		101.8	86.2	15.6	25.05	206.52	11.0
89	4/1/95	ave. $R=13.1\pm 2.4$	102.0	86.3	15.6	26.33	232.86	11.1
90	4/8/95		102.1	86.5	15.6	24.04	256.90	11.2
91	4/15/95		102.4	86.6	15.8	25.41	282.30	11.3
92	4/22/95		102.5	86.7	15.9	27.90	310.20	11.4
93	4/28/95		102.7	86.8	15.8	29.53	339.73	11.5
94	5/6/95		102.8	87.0	15.8	25.62	365.35	11.5
95	5/13/95		102.9	87.1	15.8	27.36	392.71	11.6
96	5/20/95		103.0	87.2	15.9	26.04	418.75	11.7
97	5/27/95		103.2	87.3	15.9	26.66	445.41	11.7
98	6/2/95		103.4	87.4	15.9	30.33	475.74	11.8
99	6/9/95		103.4	87.6	15.9	33.48	509.22	11.8
100	6/16/95		103.5	87.8	15.7	30.20	539.42	11.9
101	6/24/95		103.7	87.8	15.9	25.14	564.57	11.9
102	7/1/95		103.7	87.9	15.9	30.71	595.28	11.9
103	7/11/95		103.8	87.9	15.9	26.56	621.83	12.0
104	7/15/95	redrilled hole				26.59	648.43	
105	7/22/95	pump repaired	103.9	88.1	15.8	27.89	676.32	12.0
106	7/28/95		104.0	87.9	16.1	28.20	704.52	12.0
107	8/5/95		104.0	88.3	15.7	29.73	734.25	12.0
108	8/11/95		104.1	88.1	16.0	28.01	762.26	12.1
109	8/18/95		104.2	88.4	15.8	29.68	791.94	12.1
110	8/26/95		104.4	88.5	15.9	27.94	819.88	12.1
111	9/1/95		104.5	88.6	15.9	27.28	847.16	12.1
112	9/9/95		104.6	88.7	15.9	26.95	874.11	12.1
113	9/16/95		104.8	88.8	15.9	31.24	905.35	12.1
114	9/23/95		104.8	88.9	15.9	31.31	936.66	12.1
115	9/30/95		104.8	89.1	15.7	30.43	967.09	12.1
116	10/7/95		104.9	89.1	15.8	28.74	995.84	12.1
117	10/14/95		105.0	89.2	15.8	30.28	1026.1	12.1
118	10/21/95					30.74	1056.9	
119	10/28/95					37.37	1094.2	
120	11/4/95	pump replaced	105.2	89.3	15.9	45.42	1139.6	12.1
121	11/10/95		105.5	89.3	16.2	60.14	1199.8	12.1
122	11/17/95	we arrive	105.5	89.7	15.8	60.41	1260.2	12.1
123	11/24/95		105.8	89.9	15.9	49.72	1309.9	12.0
124	12/1/95		105.9	90.0	16.0	53.25	1363.2	12.0
125	12/8/95	2nd hole done	106.1	90.2	15.9	55.41	1418.6	12.0
126	12/15/95	2 collections	106.2	90.3	15.9	58.89	1477.5	11.9
127	12/22/95		106.3	90.5	15.9	59.10	1536.6	11.9
128	12/29/95	6 collections	106.5	90.6	15.9	65.86	1602.4	11.9

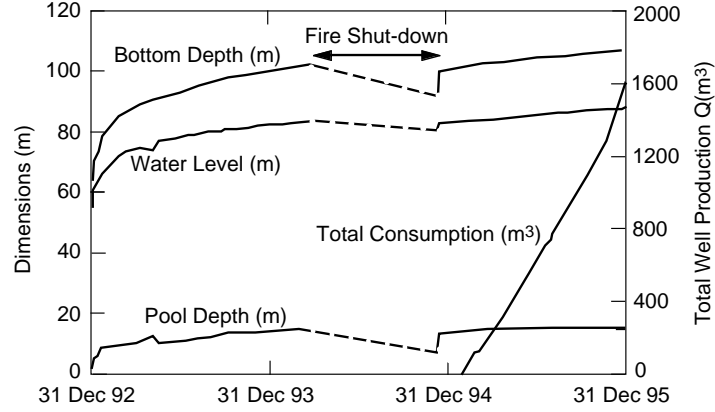


Figure A1. Measured SPWW dimensions and water consumption.

Assuming that the shape factor α is approximately constant as the well develops, the change in pool volume becomes

$$dV_p = 2\alpha HRdR + \alpha R^2 dH \quad (A6)$$

Inserting eq A6 into eq A4 yields

$$dQ = \gamma_p \pi R^2 dL - (1 - \gamma_p) (2\alpha HRdR + \alpha R^2 dH) . \quad (A7)$$

Because water consumption, water levels, and pool depths were measured, we may use eq A7 to determine pool radius throughout well development. Note that the specific gravity of ice increases approximately linearly with depth over the pool depths of interest (Kuivinen et al. 1982):

$$\gamma_p = 0.68 + 0.0028(D_p - 60) , \quad (A8)$$

where D_p is the average pool depth in meters.

Measurement uncertainties in dL and dH and slight timing differences between these measurements and those for dQ can yield unrealistic values of R if eq A7 is

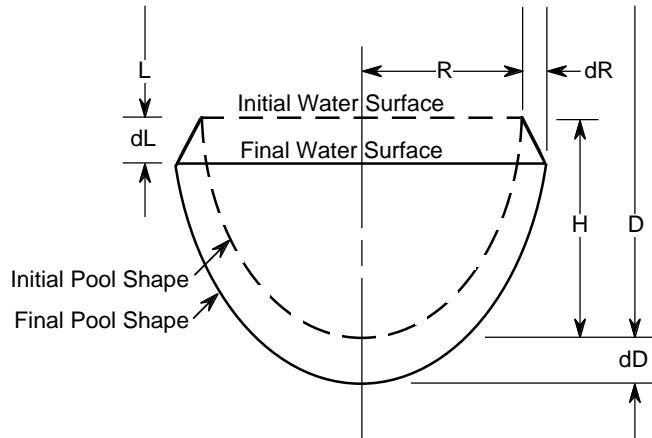


Figure A2. Schematic of well pool, showing changes in dimensions as the pool deepens.

solved for each set of values in Table A1. Instead, we generated polynomial curves that give very good fits to the data and reduce the influence of uncertainties in these measurements.

There are three periods of interest:

1. From initial startup on 12/8/92 to the fire-induced shutdown on 3/1/94,
2. From restart on 12/2/94 to the start of consumption on 1/30/95, and
3. The period of consumption ending 12/29/95 after our six collector deployments.

Periods 1 and 2

For the first two periods, no consumption occurred. Setting $dQ = 0$ and using the substitution $x = D - 60$, eq A7 becomes

$$\frac{dR}{dx} = c(x)R(x), \quad (A9)$$

where

$$c(x) = \frac{\left(\pi \frac{\gamma_p}{1-\gamma_p} \frac{dL}{dx} - \alpha \frac{dH}{dx} \right)}{2\alpha H(x)}.$$

The solution of eq A9 is simply

$$R(x) = R_0 \exp\left(\int_0^x c(x) dx \right), \quad (A10)$$

where $R_0 = R(0)$.

Figure A3 shows the measured water levels and a third-degree polynomial approximation for $L(x)$ over period 1. Note that $H(x) = x + 60 - L(x)$. Figure A4 shows the resulting solution for $\alpha = 2\pi/3$ and $R_0 = 15$ cm (the radius of the hot-water drill) plotted as $R(L)$. This curve represents the predicted shape of the well cavity formed

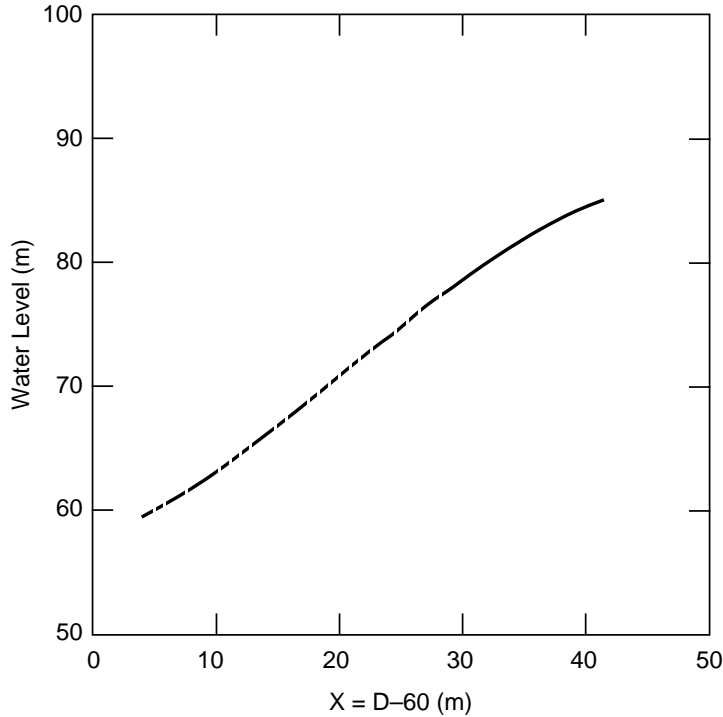


Figure A3. Period 1 (prefire) water level vs. depth and third-degree polynomial curve fitted to data.

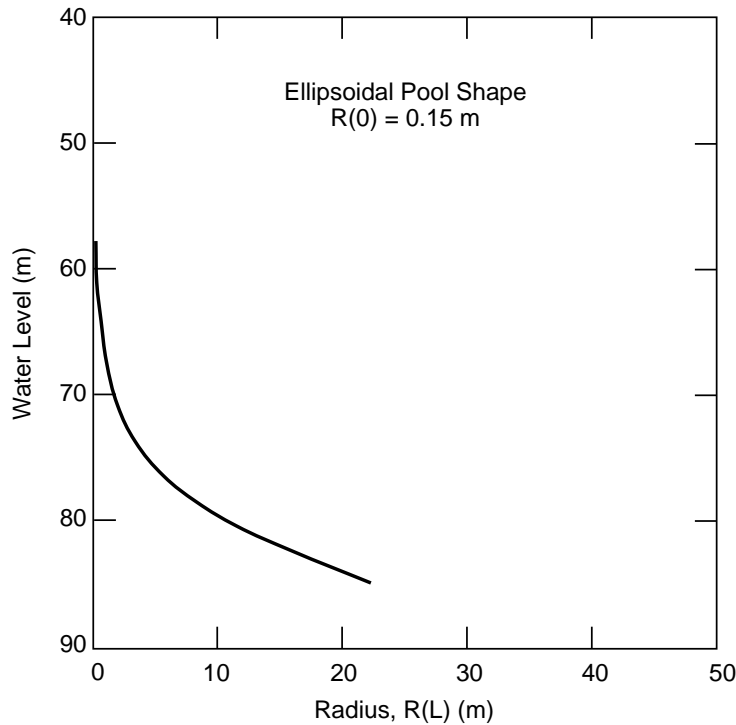


Figure A4. Predicted period 1 cavity shape, from eq A10.

during period 1. There are two main problems with these results. First, the predicted radius at the level of the freeze-back ice cover, $R(82.6 \text{ m}) = 16 \text{ m}$, is substantially larger than that estimated from down-hole video images ($8 \pm 2 \text{ m}$). Second, the observed cavity appeared to flare out at its upper end and become more vertical toward its bottom; that is, it appeared to be bell-shaped. The predicted shape actually has the opposite trend: it is narrow (with near vertical walls) at its upper end, and it flares out towards the bottom.

The most likely cause for the poor prediction by eq A10 is that it does not account for water percolation out of the well ($dQ \neq 0$ in eq A7). Based on other Rodriguez wells, Lunardini and Rand (1995) assumed that percolation would cease at an ice specific gravity greater than 0.72, corresponding to depths below 74 m. This generally agrees with Williams (1974), who expected that percolation from the first South Pole Rodriguez well would cease at about 76 m. Modeling the percolation from the well is beyond the present scope of work and would introduce its own uncertainties. A more satisfactory approach would be to measure the cavity radius as a function of depth using a device lowered into the well.

Period 2 covers the two-month period after restarting the well on 12/2/94 but before consumption began on 1/30/95. The well had frozen back about 11 m during the nine-month shut down after the fire. Although percolation would not be significant during period 2, new ice had not been melted before the start of consumption. That is, there is no need to analyze period 2 to determine the volume of ice melted that released micrometeorites into the well.

Period 3

During the period of water consumption, the water level was below 85 m, and we would expect percolation to be zero. Thus, eq A7 may be used to relate changes in well dimensions to the rate of water consumed. Figure A5 shows the polynomial curves fitted to L , H , and Q data for period 3 (with $x = D - 100.5$). Note that dH/dx

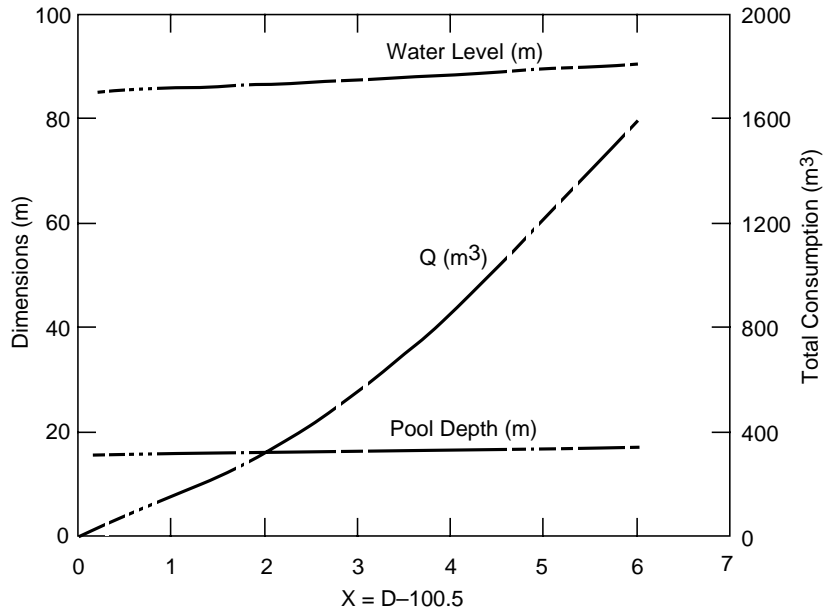


Figure A5. Period 3 (consumption) dimensions and water consumption, and polynomial curves fitted to data.

over the period is less than 0.1, so we may treat H as a constant for the period, $H = 15.5$ m. In addition, solution of eq A7 requires an integration constant. If we assume that changes in well radius become small near the end of the period (i.e., the well dimensions stabilize) we may solve eq A7 with $dR/dx = 0$ to obtain an integration constant, $R(6 \text{ m}) = 11.9$ m.

Figure A6 shows the resulting prediction for the $R(L)$ obtained by solving eq A7

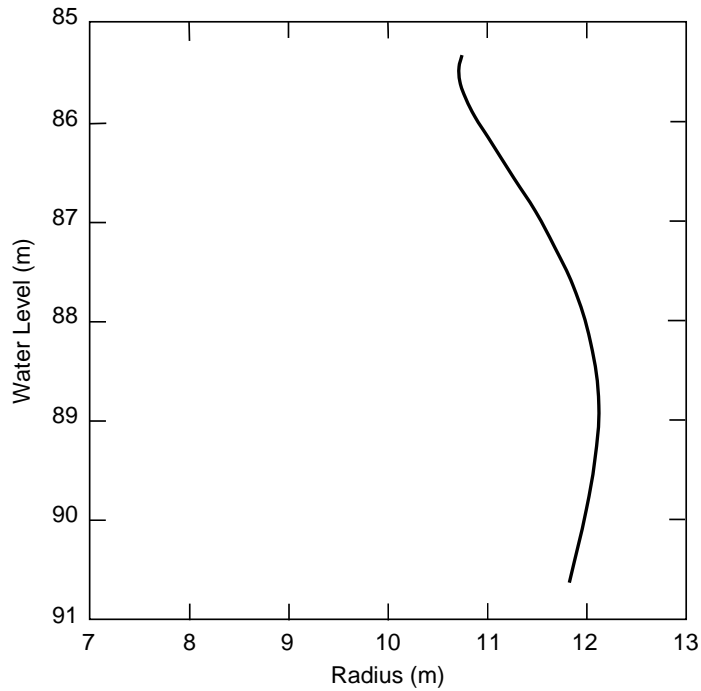


Figure A6. Predicted period 3 cavity shape, from eq A7.

for both ellipsoid and paraboloid pool shapes and averaging the results (radii differences due to pool shape are less than about 30 cm). Note that the predicted radius of 11.1 m at $L = 86.3$ m agrees with the results of the draw-down tests conducted in March/April 1995, $R = 13.1 \pm 2.4$ m.

Composite well shape

We may use the foregoing analyses to compose our best estimate of the well shape at the end of our collector deployments in December 1995. For the period of water consumption, eq A7 provides a reasonable estimate for the cavity shape. In addition, shape data from previous Rodriguez wells and our own video records from the SPWW indicate that an ellipsoidal pool shape is reasonable for the below-water portion of the well. Unfortunately, by not accounting for percolation, eq A7 yields an unrealistic shape for the prefire well cavity. Therefore, for period 1 (and the short period 2) we will estimate cavity shape by using an approximation adopted by Lunardini and Rand (1995): the ratio of pool radius/depth is approximately constant. This ratio for period 3 ranges from 0.69 to 0.77 and averages 0.74. We used

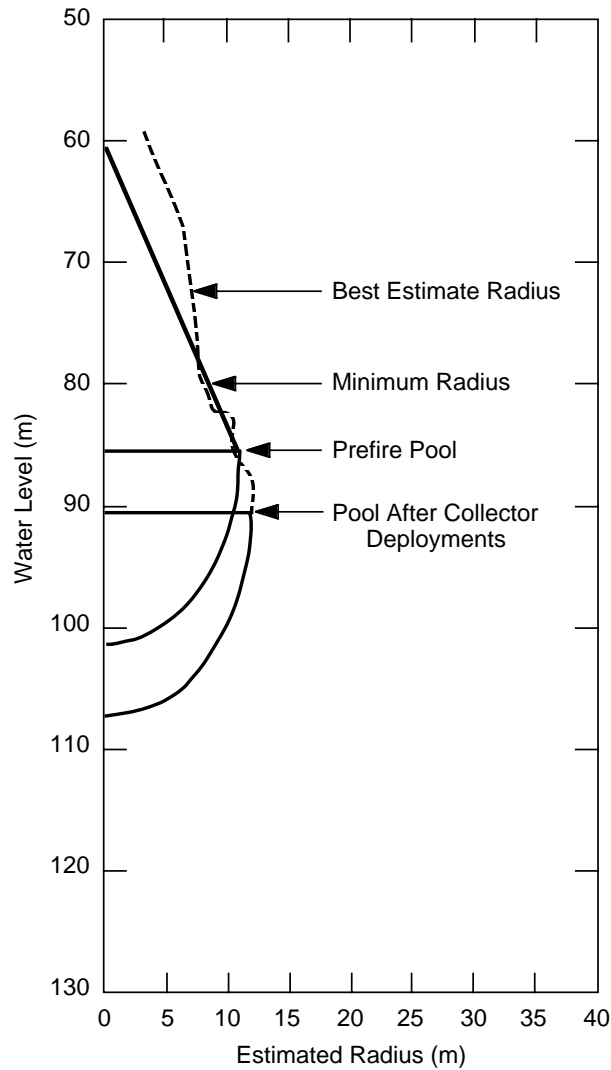


Figure A7. Composite well shape, showing two possible prefire cavity shapes.

its value at the start of consumption, $R/H = 0.70$, to ensure that the well shape is continuous at the transition from period 2 to period 3.

Figure A7 shows the resulting composite well shape. Use of $R/H = 0.70$ for period 1 yields a bell-shaped cavity that is qualitatively consistent with the observed shape. It predicts a radius of 10 m at the level of the freeze-back ice cover, consistent with the observed value of 8 ± 2 m. However, $R/H = 0.70$ probably overpredicts the cavity size near its upper level. Thus, Figure A7 shows a conical wall shape that should underpredict the prefire cavity size. Figure A7 also shows ellipsoidal pools as they would have existed immediately before the 1994 fire and just following our 1995 collector deployments.

Ice volume and mass melted

We may use Figure A7 to estimate the volume and mass of ice melted that contributed micrometeorites to the well. The prefire cavity volume ranges between $3,300 \text{ m}^3$ and $4,400 \text{ m}^3$ for the conical and $R/H = 0.70$ shapes, respectively. Using the average value and applying a 20% uncertainty, we estimate the prefire ice volume melted as $3,900 \pm 800 \text{ m}^3$. The period 3 analysis yields a cavity volume of $2,200 \text{ m}^3$ with an ellipsoidal pool of $4,700 \text{ m}^3$. Assuming $\pm 10\%$ uncertainty, the period 3 ice volume melted is $6,900 \pm 700 \text{ m}^3$. Combining these values yields a total volume of ice melted as $11,000 \pm 1,000 \text{ m}^3$. Accounting for the variation of density with depth, we estimate the total ice mass melted as $8,100 \pm 900$ tonnes.

APPENDIX B: SUMMARY OF COLLECTOR DEVELOPMENT TESTS.

<i>Date</i>	<i>Collector test facility</i>	<i>Mat'l added (g)</i>	<i>Mat'l recovered (g)</i>	<i>Percent recovered</i>	<i>Type of material</i>	<i>Remarks</i>
14 May	1 ft	100	71.07	71.07	Mixture A	Fines from aolian sample were not recovered, they did not plug the filter.
16 May	1 ft	200	165.6	82.80	Ss 297–420 μm	Particles were flushed out of collector by water draining through slot.
24 May	1 ft	200	191.6	95.80	Ss 200–400 μm	Tried polyethylene check valve
30 May	1 ft	100	78.81	78.81	Ss 200–400 μm Bg 75–150 μm	Check valve not tight
29 Jun	4-ft tank	390.1	387	99.21	Ss 200–400 μm Bg 75–150 μm	Rough ice, multiple passes
30 Jun	4-ft tank	100.1	99.54	99.44	Ss 200–400 μm Bg 75–150 μm	Smooth ice 50 g, rough ice 50 g
6 Jul	4-ft tank	100	99.46	99.46	Ss 200–400 μm Bg 75–150 μm	Smooth ice 50 g, rough ice 50 g
10 Jul	4-ft tank	231.51	206.38	89.15	Mixture B	Rough ice surface
23 Aug	4-ft basin				Ss 200–400 μm Bg 75–150 μm	Could see sweep line of collector
6 Sep	4-ft tank					Outer flap picked up particles extremely well.
24 Aug	8-ft basin					Needs weight in center
28 Aug	8-ft basin				Bg >400 μm	

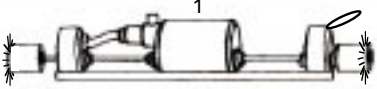
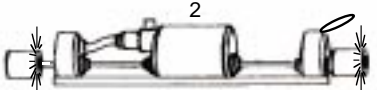
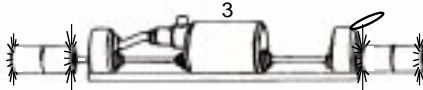
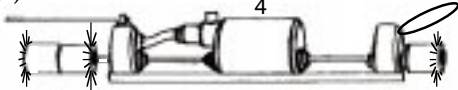
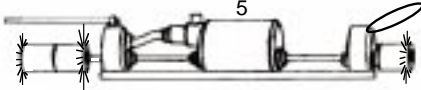
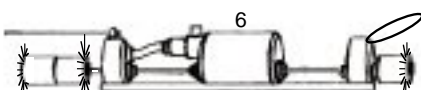
Ss = Silica sand.

Bg = Black glass.

Mixture A: 50 g Antarctic aeolian dust, 49 g silica sand 297–420 μm, 1 g metal, and glass spheres 50–400 μm size.

Mixture B: 68 g silica sand 200–400 μm, 20 g black glass 150–425 μm, 8 g stainless steel spheres 60–125 μm, and 4 g black glass 75–150 μm.

APPENDIX C: SUMMARY OF COLLECTOR DEPLOYMENTS IN SPWW.

<i>Date</i>	<i>Deployment no./ area collected</i>	<i>Configuration</i>	
14 Dec	1 Pocket 1	Single weights on short shaft Small hubs on outside of weights Small hanging hoop	
15 Dec	2 Pocket 1 & 2	Single weights on short shafts Large hub, 6.25 ≤ O.D. on inside of weight on lower end, outside on upper end Small hanging hoop	
18 Dec	3 Plateau only	Double weights on both shafts Small hubs outside, large inside Small hanging hoop	
22 Dec	4	Double weight on long (lower) shaft Large hanging hoop Sting motors failed	
23 Dec	5 Pocket 5	Double weight on long (lower) shaft Large hanging hoop Sting	
25 Dec	6 Pocket 6	Double weight on long (lower) shaft Large hanging hoop Sting	

REPORT DOCUMENTATION PAGE

Form Approved
OMB No. 0704-0188

Public reporting burden for this collection of information is estimated to average 1 hour per response, including the time for reviewing instructions, searching existing data sources, gathering and maintaining the data needed, and completing and reviewing the collection of information. Send comments regarding this burden estimate or any other aspect of this collection of information, including suggestion for reducing this burden, to Washington Headquarters Services, Directorate for Information Operations and Reports, 1215 Jefferson Davis Highway, Suite 1204, Arlington, VA 22202-4302, and to the Office of Management and Budget, Paperwork Reduction Project (0704-0188), Washington, DC 20503.

1. AGENCY USE ONLY (Leave blank)		2. REPORT DATE May 1997	3. REPORT TYPE AND DATES COVERED	
4. TITLE AND SUBTITLE Collecting Micrometeorites from the South Pole Water Well			5. FUNDING NUMBERS	
6. AUTHORS Susan Taylor, James H. Lever, Ralph P. Harvey, and John Govoni				
7. PERFORMING ORGANIZATION NAME(S) AND ADDRESS(ES) U.S. Army Cold Regions Research and Engineering Laboratory 72 Lyme Road Hanover, New Hampshire 03755-1290			8. PERFORMING ORGANIZATION REPORT NUMBER CRREL Report 97-1	
9. SPONSORING/MONITORING AGENCY NAME(S) AND ADDRESS(ES) National Science Foundation Arlington, Virginia 22230			10. SPONSORING/MONITORING AGENCY REPORT NUMBER	
11. SUPPLEMENTARY NOTES				
12a. DISTRIBUTION/AVAILABILITY STATEMENT Approved for public release; distribution is unlimited. Available from NTIS, Springfield, Virginia 22161			12b. DISTRIBUTION CODE	
13. ABSTRACT (<i>Maximum 200 words</i>) A collector was designed and built to retrieve micrometeorites from the floor of the South Pole Water Well. The large volume of firm and ice being melted for the well and the low component of terrestrial material in Antarctic ice make the South Pole Water Well an ideal place to collect micrometeorites. Because the age of the ice being melted is known, yearly or periodic collections provide large numbers of micrometeorites of known terrestrial age. The collector was designed to pose no threat to the well's water quality, to be reliable and easy to operate, and to collect particles larger than 50 μm . This report details how this collector was built and tested and documents the rationale behind some of the design choices. It also includes preliminary findings from the first deployment.				
14. SUBJECT TERMS Antarctica Cosmic dust Micrometeorites South Pole Water well			15. NUMBER OF PAGES 42	
			16. PRICE CODE	
17. SECURITY CLASSIFICATION OF REPORT UNCLASSIFIED	18. SECURITY CLASSIFICATION OF THIS PAGE UNCLASSIFIED	19. SECURITY CLASSIFICATION OF ABSTRACT UNCLASSIFIED	20. LIMITATION OF ABSTRACT UL	